A QUANTUM TRACE MAP FOR 3-MANIFOLDS

STAVROS GAROUFALIDIS AND TAO YU

Abstract. We define a quantum trace map from the skein module of a 3-manifold with torus boundary components to a module (left and right quotient of a quantum torus) constructed from an ideal triangulation. Our map is a 3-dimensional version of the well-known quantum trace map on surfaces introduced by Bonahon and Wong and further developed by Lê.

Contents

Date: 19 March 2024.

Keywords and phrases: Kauffman bracket skein module, 3-manifolds, knots, character varieties, quantum trace map, ideal triangulations, gluing equations, quantum gluing module, Frobenius-Chebyshev homomorphism.

1. Introduction

1.1. **The quantum trace map of a surface.** The quantum trace map, introduced by Bonahon–Wong [BW11] connects the skein algebra of a punctured surface (a quantum object), with an algebra of q-commuting variables related to hyperbolic geometry. The quantum trace map was originally introduced as a replacement of the topologically defined skein module (generated by framed links) and the algebro-geometric quotient of the character variety of a surface group by a more manageable object, namely a quantum torus, i.e., a Laurent polynomial ring of q-commuting variables. The original discovery of Bonahon–Wong used miraculous cancellations which have seen been explained by subsequent work of Lê [Lê15]. This map has recently attracted a lot of attention from researchers in topology, representation theory, character varieties, cluster algebras and their quantization.

Recall that the skein module of a closed oriented surface $S(\Sigma)$ (with coefficients in a ring R that contains an invertible element q) is the R-module generated by the set of isotopy classes of framed unoriented links in $\Sigma \times (-1,1)$, modulo the relations (1) and (2).

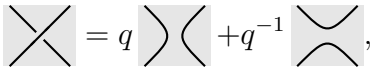

(1)

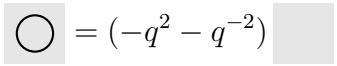

(2)

The skein module was introduced in the early days of quantum topology by Przytycki [Prz91] and Turaev [Tur88].

There is a well-known connection between the skein module of a surface (or an arbitrary 3-manifold) and the $\mathrm{SL}_2(\mathbb{C})$-character variety. Namely, when $q = 1$, the skein module $\mathcal{S}_1(\Sigma)$ is a commutative algebra whose quotient by its nil radical coincides with the coordinate ring of the $\mathrm{SL}_2(\mathbb{C})$-character variety of Σ. The quantum trace map sends the skein module $\mathcal{S}_1(\Sigma)$ to a quantum torus that depends on an ideal triangulation of Σ. Two key features of this map are

(a) The skein module $\mathcal{S}(\Sigma)$ of Σ is an associative (and in general non-commutative) algebra, and so is the target quantum torus.
(b) The quantum trace map depends on an ideal triangulation of Σ, but it is invariant under 2–2 Pachner moves that connect any two such triangulations. The reason behind this is the fact that the $\mathrm{SL}_2(\mathbb{C})$-character variety of irreducible representations of a surface is irreducible and has canonical coordinates induced by an ideal triangulation of the surface.

Our aim is to define a 3-dimensional analogue of the quantum trace map for a 3-manifold M equipped with an ideal triangulation $\mathcal{T}$. Unfortunately the two key features above fail for

3-manifolds. Indeed, the domain of such a map, namely the skein module $\mathcal{S}(M)$, is no longer an algebra but only a module over a universal coefficient ring (and in general only a module over the skein algebra $\mathcal{S}(\partial M)$ of the boundary of M). Likewise, as in the case of a surface, an ideal triangulation $\mathcal{T}$ gives coordinates for some components of the $\mathrm{SL}_2(\mathbb{C})$-character variety of irreducible representations of M. But now, this variety contains several components, some of which are detected by an ideal triangulation $\mathcal{T}$, but these detected components are no longer invariant under 2–3 Pachner moves that connect every two ideal triangulations.

With these subtleties in mind, we define a 3-dimensional quantum trace map that allows one to do computations using the standard methods of 3-manifold triangulations developed in `SnapPy` [CDGW].

1.2. **Preliminaries.** To define the 3-dimensional quantum trace map we will fix an oriented 3-manifold M and an ideal triangulation $\mathcal{T}$ of it. The boundary of the manifold can be arbitrary, however the most important case for us will be the case where the boundary is a finite union of tori, for instance when M is the complement of a knot in 3-space. There are three ingredients that go into the definition.

- The gluing equations variety $G_{\mathcal{T}}$.
- The coordinate ring $\mathbb{C}[X_M^{\mathrm{Fr}}]$ of $\mathrm{SL}_2(\mathbb{C})$-character variety of X_M^{Fr}.
- The quantum torus $\mathbb{T}(\mathcal{T})$ and its left/right quotient $\widehat{\mathcal{G}}(\mathcal{T})$.

We will begin by giving a brief description of what is needed here, and refer to the later sections for a detailed discussion. We first recall the gluing equations variety of an ideal triangulation introduced by Thurston [Thu97] and further studied by Neumann–Zagier [NZ85]. Fix a connected, oriented 3-manifold M with torus boundary components and an ideal triangulation $\mathcal{T}$ of M that consists of N tetrahedra $T_1, \dots, T_N$. Note that the number of edges of $\mathcal{T}$ is also N. We can assign shape parameters Z_j, $Z'_j = 1/(1-Z_j)$ and $Z''_j = 1 - 1/Z_j$ to each pair of opposite edges of the ideal tetrahedron T_j, where the triple (Z_j, Z'_j, Z''_j) satisfies the equations

$$Z_j Z'_j Z''_j = -1, \qquad Z_j + Z_j'^{-1} = 1, \qquad Z'_j + Z_j''^{-1} = 1, \qquad Z''_j + Z_j^{-1} = 1\,. \tag{3}$$

Each edge e of $\mathcal{T}$ gives rise to a gluing equation

$$\prod_{T:\, e \in T} Z_T^{\square} = 1 \tag{4}$$

given as the product of the shapes of the tetrahedra that go around the edge.

The gluing equations variety $G_{\mathcal{T}}^P$ is defined as the solutions in $(\mathbb{C}^\times)^{3N}$ of all shapes $Z = (Z_1, Z'_1, Z''_1, \dots, Z_N, Z'_N, Z''_N)$ that satisfy the Lagrangian equations (3) for $j = 1, \dots, N$ and all the edge gluing equations (4). A point in the gluing equations variety $G_{\mathcal{T}}^P$ gives a $\mathrm{PSL}_2(\mathbb{C})$-representation of $\pi_1(M)$, well-defined up to conjugation (thus the superscript P in $G_{\mathcal{T}}^P$). Said differently, an ideal triangulation gives a chart for the $\mathrm{PSL}_2(\mathbb{C})$-character variety of the manifold.

However, we need a lift of the theory to $\mathrm{SL}_2(\mathbb{C})$. To achieve this, we assign square root shape parameters z_j, z'_j, z''_j to pairs of opposite edges of each tetrahedron T_j. These parameters satisfy the following equations

$$z_j z'_j z''_j = \mathbf{i}, \qquad z_j^2 + (z'_j)^{-2} = 1, \qquad (z'_j)^2 + (z''_j)^{-2} = 1, \qquad (z''_j)^2 + z_j^{-2} = 1 \tag{5}$$

and the edge equations which take the form

$$\prod_{T:\, e\in T} z_T^{\square} = -1\,. \tag{6}$$

As before, the gluing equations variety $G_{\mathcal{T}}$ is defined as the solutions in $(\mathbb{C}^\times)^{3N}$ of all shapes $z = (z_1, z_1', z_1'', \dots, z_N, z_N', z_N'')$ that satisfy the Lagrangian equations (5) for $j = 1, \dots, N$ and all the edge gluing equations (6). With this twist, a point in the gluing equations variety $G_{\mathcal{T}}$ gives an $\mathrm{SL}_2(\mathbb{C})$-representation of $\pi_1(X_M^{\mathrm{Fr}})$ of the oriented framed bundle X_M^{Fr} of M; see Proposition 3.3. At the same time, the specialization to $q = 1$ of the skein module $\mathcal{S}(M)$, divided by the nilradical, coincides with the coordinate ring of X_M^{Fr}; see Lemma 4.2 below.

The last ingredient that we now discuss is the quantum torus and its two-sided quotient, the gluing equations module. As in the skein module of M, we fix a ring R that contains an invertible element $q^{1/2}$ and a primitive 4-th root of unity $\mathbf{i}$. Associated to $\mathcal{T}$ is a quantum torus

$$\mathbb{T}(\mathcal{T}) = \bigotimes_{j=1}^{N} \mathbb{T}\langle \hat z_j, \hat z_j''\rangle, \qquad \mathbb{T}\langle \hat z_j, \hat z_j''\rangle = R\langle \hat z_j, \hat z_j''\rangle / \langle \hat z_j'' \hat z_j - q \hat z_j \hat z_j''\rangle \tag{7}$$

where the variables $\hat z_j$ and $\hat z_\ell''$ for $j, \ell = 1, \dots, N$ commute except in the following instance $\hat z_j \hat z_j'' = q \hat z_j'' \hat z_j$. A more symmetric definition of $\mathbb{T}\langle \hat z_j, \hat z_j''\rangle$ is given by the quotient of $R\langle \hat z_j, \hat z_j', \hat z_j''\rangle$ where the three variables satisfy the q-commutation relations

$$\hat z_j \hat z_j' = q \hat z_j' \hat z_j, \qquad \hat z_j' \hat z_j'' = q \hat z_j'' \hat z_j', \qquad \hat z_j'' \hat z_j = q \hat z_j \hat z_j'', \qquad \hat z_j \hat z_j' \hat z_j'' = \mathbf{i} q^{3/2}\,. \tag{8}$$

The quantum torus $\mathbb{T}(\mathcal{T})$ is an associative algebra and has a left and a right ideal generated, respectively, by the Lagrangian equations

$$\hat z_j^{-2} + (\hat z_j'')^2 = 1 \tag{9}$$

for $j = 1, \dots, N$ and by the edge gluing equations

$$\prod_{T:\, e\in T} \hat z_T^{\square} = -q^2 \tag{10}$$

for all edges, where the product of these q-commuting variables is given by their canonical Weyl-ordering (see Section 4.8 below).

The *quantum gluing equations module* $\widehat{\mathcal{G}}(\mathcal{T})$ is the quotient of $\mathbb{T}(\mathcal{T})$ from the left by the edge-equations and from the right by the Lagrangian equations

$$\widehat{\mathcal{G}}(\mathcal{T}) = \langle \text{edge}\rangle_R \backslash \mathbb{T}(\mathcal{T}) /_L \langle \text{Lagrangian}\rangle\,. \tag{11}$$

The quantum gluing equations module is implicit in the work of Dimofte who studied the quantization of the character variety of an ideally-triangulated 3-manifold [Dim13]. Dimofte used the symplectic properties of the gluing equations (coming from the symplectic properties of the Neumann–Zagier matrices), as well as standard methods of non-commutative symplectic reduction to arrive at a module of q-commuting operators. A similar module appears in [AGLR, Eqn.(10)].

Our definition of $\widehat{\mathcal{G}}(\mathcal{T})$ comes from a presentation of the skein module of M as a quotient by a left and by a right ideal (see Proposition 1.2 below), which itself comes from the fact

that the 3-manifold M is obtained by a thickened surface by attaching 2-handles on either side.

1.3. **Our results.** We now have all the ingredients to phrase our main result. Fix an ideal triangulation $\mathcal{T}$ of a 3-manifold M as above.

Theorem 1.1. *There exists a map*

$$\widehat{\mathrm{tr}} : \mathcal{S}(M) \longrightarrow \widehat{\mathcal{G}}(\mathcal{T}) \tag{12}$$

that fits in a commutative diagram

$$\begin{array}{ccc} \mathcal{S}(M) & \longrightarrow & \widehat{\mathcal{G}}(\mathcal{T}) \\ \downarrow & & \downarrow \\ \mathbb{C}[X_M^{\mathrm{Fr}}] & \longrightarrow & \mathbb{C}[G_{\mathcal{T}}] \end{array} . \tag{13}$$

The left vertical map was already discussed. The quantum trace map (12) is given by the composition

$$\mathcal{S}(M) \xleftarrow{\cong} \langle B\rangle_R \backslash \mathcal{S}(\Sigma_{\mathcal{T}}) /_L \langle A\rangle \longrightarrow \widehat{\mathcal{G}}(\mathcal{T}). \tag{14}$$

Here, $\Sigma_{\mathcal{T}}$ is the boundary of a small neighborhood of the dual 1-skeleton of $\mathcal{T}$, and it is decorated with two sets of curves $\{A_f\}, \{B_e\}$ that bounds disks in M but not $\Sigma_{\mathcal{T}}$. The kernel of the natural map $\mathcal{S}(\Sigma_{\mathcal{T}}) \to \mathcal{S}(M)$ includes handle slides along these curves, discussed in detail in Section 4.1 below. Let ${}_L\langle A\rangle$ and $\langle B\rangle_R$ denote the submodule generated by handle slides along the corresponding types of curves.

Proposition 1.2. ${}_L\langle A\rangle$ and $\langle B\rangle_R$ are left and right ideals in $\mathcal{S}(\Sigma_{\mathcal{T}})$ respectively, and we have an isomorphism of R-modules

$$\mathcal{S}(M) \cong \langle B\rangle_R \backslash \mathcal{S}(\Sigma_{\mathcal{T}}) /_L \langle A\rangle \,. \tag{15}$$

The reason behind the isomorphism (15) is topological, namely the manifold M is obtained from the thickened surface $\Sigma_{\mathcal{T}} \times [-1, 1]$ by attaching A-handles on one side and B-handles on the other.

The identification (15) is a convenient way to encode elements of the 3d-skein module $\mathcal{S}(M)$ in coordinates. Aside from its use in the 3d-quantum trace map, the above coordinate presentation of the skein module of a 3-manifold is useful computationally and also theoretically. Indeed, several quantum invariants, such as the Witten–Reshetikhin–Turaev invariant and its lift to the Habiro ring, the state integrals of Andersen–Kashaev and the 3D-index of Dimofte–Gaiotto–Gukov can be extended to invariants of the skein module of M and factor through the quantum trace map. We will discuss this topic in a subsequent publication.

We next discuss the quantum trace map when $q = \zeta$ is a root of unity. More precisely, we fix a root of unity ζ such that ζ^4 is a primitive N-th root of unity, and let $\varepsilon = \zeta^{N^2}$, a 4-th root of unity. In this case, we denote the skein module and the quantum gluing equations module by $\mathcal{S}_\zeta(M)$ and $\widehat{\mathcal{G}}_\zeta(\mathcal{T})$, and their classical versions by $\mathcal{S}_\varepsilon(M)$ and $\widehat{\mathcal{G}}_\varepsilon(\mathcal{T})$ to indicate the dependence on the chosen root of unity.

In this case, both the skein and the quantum gluing equations modules have a Chebyshev-Frobenius homomorphism

$$\Phi_\zeta : \mathcal{S}_\varepsilon(M) \to \mathcal{S}_\zeta(M), \qquad \varphi_\zeta : \widehat{\mathcal{G}}_\varepsilon(\mathcal{T}) \to \widehat{\mathcal{G}}_\zeta(\mathcal{T}) \tag{16}$$

where the former is defined geometrically by threading a framed link by a linear combination of parallels given by the N-th Chebyshev polynomial, and the latter is defined algebraically on a quantum torus by raising its generators to their N-th powers. In both cases, the quantum binomial theorem and the vanishing of the quantum binomial at roots of unity imply that both maps (16) are well-defined. This is discussed in detail in Section 5.4 below.

The two maps (16) are related by the quantum trace, which is analogous to the surface case [BL22, Theorem 5.2].

Theorem 1.3. *The following diagram commutes.*

$$\begin{array}{ccc} \mathcal{S}_\varepsilon(M) & \xrightarrow{\widehat{\mathrm{tr}}^{\varepsilon}_{\mathcal{T}}} & \widehat{\mathcal{G}}_\varepsilon(\mathcal{T}) \\ \downarrow{\scriptstyle \Phi_\zeta} & & \downarrow{\scriptstyle \varphi_\zeta} \\ \mathcal{S}_\zeta(M) & \xrightarrow{\widehat{\mathrm{tr}}^{\zeta}_{\mathcal{T}}} & \widehat{\mathcal{G}}_\zeta(\mathcal{T}) \end{array} . \tag{17}$$

We finally discuss the issue of effective computation. An important feature of the quantum trace map (12) is that it is effectively computable. In fact, it is computable by the same methods of `SnapPy` pioneered by Thurston and developed by Weeks (and more recently, by Culler, Dunfield and Goerner [CDGW]) to study hyperbolic structures of 3-manifolds and their deformations. For a detailed discussion, see Section 6.

1.4. **Further directions.** We end this section with some brief comments about further directions. As mentioned already, ideal triangulations are related by a sequence of 2–3 Pachner moves. However, even classically, the gluing equations variety $G_{\mathcal{T}}$ "sees" some components of representations of the framed manifold, and these components can change under 2–3 Pachner moves. Hence, the codomain $\widehat{\mathcal{G}}(\mathcal{T})$ of the quantum trace map can change under 2–3 Pachner moves, and what is worse, it can become trivial when $\mathcal{T}$ is a degenerate ideal triangulation (e.g., has a univalent vertex). Hence, the map (13) is *not* invariant under 2–3 Pachner moves. On the other hand, the map is invariant under 3–2 Pachner moves, and under certain conditions, also invariant under 2–3 moves. We postpone this discussion to a subsequent publication.

Finally, extensions to the SL_n-version of the quantum-trace map, building on the results of [LY] are possible and will also be discussed subsequently.

2. Triangulations

2.1. **Oriented triangulations and their dual surfaces.** In this section we recall oriented ideal triangulations, and define their dual surfaces. Let T be an oriented tetrahedron. A labeling of the vertices of T by $0, 1, 2, 3$ is compatible with the orientation if vertices $1, 2, 3$ are counterclockwise when viewed from vertex 0. We represent the tetrahedron using a top view like Figure 1.

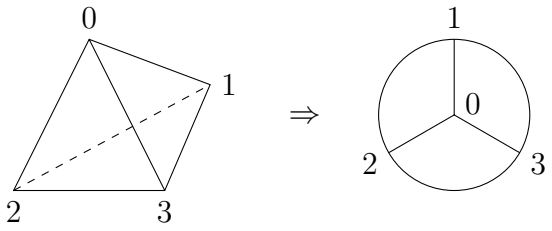

FIGURE 1. Labeling a tetrahedron.

Suppose M is a compact oriented 3-manifold with nonempty boundary. An oriented triangulation $\mathcal{T}$ of M is a collection of tetrahedra $T_1, \ldots, T_N$ whose faces are paired using orientation reversing homeomorphisms such that gluing the tetrahedra minus the vertices gives the interior of M.

As in the introduction, consider the dual 1-skeleton of $\mathcal{T}$, which is a graph embedded in M. A small neighborhood of the dual 1-skeleton is a handlebody. Then $\Sigma_{\mathcal{T}}$ is defined as the boundary of this handlebody and oriented using the outward normal. The intersection of $\Sigma_{\mathcal{T}}$ with each face f of $\mathcal{T}$ is a circle denoted A_f. There is another set of pairwise disjoint curves B_e on $\Sigma_{\mathcal{T}}$, one for each edge e of $\mathcal{T}$, such that B_e bounds a disk dual to e in the complement of the handlebody. Here, dual to e means that the disk intersects e at a point, and it does not intersect other edges. We define B_e more carefully in the following.

In a tetrahedron T, $\Sigma_{\mathcal{T}} \cap T$ is a sphere with 4 boundary components. Borrowing from the theory of mapping class groups of surfaces, we call it the *lantern*. The boundary of the lantern consists of the A-curves on the faces of the tetrahedron. Each pair of boundary curves can be connected by an arc that goes around the edges of the tetrahedron. We call these arcs the *standard arcs* on the lantern, and the lantern decorated with the standard arcs is called the *standard lantern*, denoted $\mathbb{L}$. This is shown in Figure 2, where the blue arcs are the standard arcs.

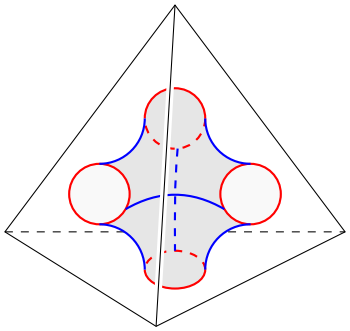

FIGURE 2. Lantern surface in a tetrahedron. A-curves in red, B-arcs in blue.

In the triangulation $\mathcal{T}$, there is an embedded copy of $\mathbb{L}$ in each tetrahedron. When a pair of faces is glued, so does the corresponding boundary components of embedded $\mathbb{L}$. The face pairing also includes how the edges of the faces are matched. Then we can require that the standard arcs dual to the matched edges connect to each other. After all faces are glued, the standard arcs form the B-circles.

The data $\mathcal{H}_{\mathcal{T}} := (\Sigma_{\mathcal{T}}, \{A_f\}, \{B_e\})$ is called the *dual surface* to the triangulation $\mathcal{T}$. We just argued that $\mathcal{H}_{\mathcal{T}}$ can be constructed from the face pairings of $\mathcal{T}$. Conversely, The intersection pattern of the curves $\{A_f\}$ and $\{B_e\}$ determines the face pairings of the triangulation. In this sense, $\mathcal{H}_{\mathcal{T}}$ is equivalent to the triangulation $\mathcal{T}$.

2.2. **Diagrams for the lantern.** The orientation of $\Sigma_{\mathcal{T}}$ is important, for example in the definition of the skein algebra. Thus, we want to describe a triangulation $\mathcal{T}$ using combinatorial data that respects orientations.

Now consider the standard lantern inside the tetrahedron. Notice that the lantern is a smooth version of the truncated tetrahedron, which is embedded in the tetrahedra of $\mathcal{T}$ in a dual position. See Figure 3, where the top view is also included. Note the dual vertex 3 is in the back, which affects the orientation of the figure. We either stretch the back vertex to infinity and truncate, or rotate the dual tetrahedron to make some vertex the top one. See Figure 4. Note the labeling is opposite of the orientation of the dual tetrahedron.

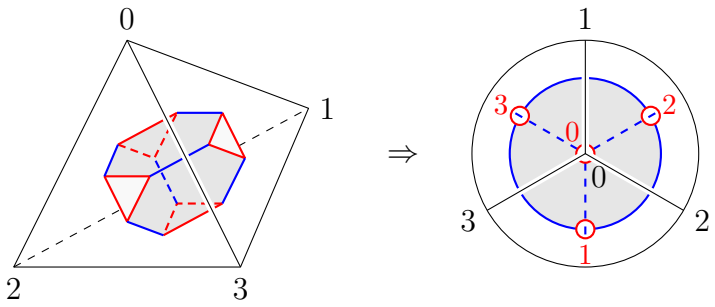

FIGURE 3. Truncated dual tetrahedron.

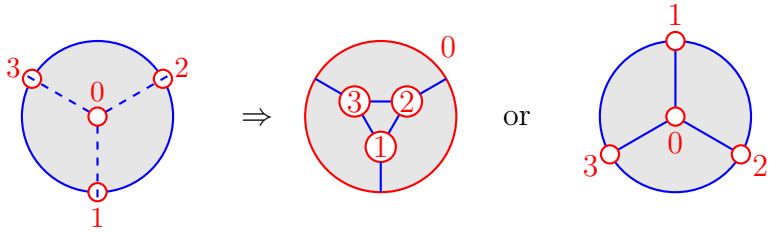

FIGURE 4. Different diagrams of the lantern.

3. Classical case

By "classical" one usually refers to the specialization $q = 1$ of the skein module, which is then related to the $\mathrm{PSL}_2(\mathbb{C})$-character variety of the ambient manifold. In this section we recall several well-known facts about triangulations and $\mathrm{SL}_2(\mathbb{C})$-character varieties of 3-manifolds. Our constructions will involve $\mathrm{SL}_2(\mathbb{C})$-representations rather than $\mathrm{PSL}_2(\mathbb{C})$ ones that come naturally from developing maps in hyperbolic geometry (due to the fact that the orientation preserving isometries of 3-dimensional hyperbolic space is $\mathrm{PSL}_2(\mathbb{C})$).

This subtle distinction between PSL_2 versus SL_2 will require minor twists and modifications of well-known results.

3.1. **Twisted character variety.** The first twist in this story is that we need to consider the frame bundle $p : \mathrm{Fr}M \to M$ of oriented orthonormal frames in the tangent bundle of M (defined with respect to some fixed Riemannian metric on M) as opposed to M itself.

This is a principal SO_3-bundle, and in dimension 3, it is well-known that it is trivial. This implies that

$$\pi_1(\mathrm{Fr}M) \cong \pi_1(M) \times \mathbb{Z}/2. \tag{18}$$

Here $\mathbb{Z}/2 \cong \pi_1(\mathrm{SO}_3)$ is canonically included in the center of $\pi_1(\mathrm{Fr}M)$ using the inclusion of the fiber $i : \mathrm{SO}_3 \hookrightarrow \mathrm{Fr}M$, whereas the inclusion of $\pi_1(M)$ depends on a spin structure of M.

Let X_M^{Fr} be the subset of the $\mathrm{SL}_2(\mathbb{C})$-character variety of $\mathrm{Fr}M$ represented by homomorphisms $\pi_1(\mathrm{Fr}M) \to \mathrm{SL}_2(\mathbb{C})$ sending a nontrivial loop in the fiber to $-I$. It is non-canonically isomorphic to the usual $\mathrm{SL}_2(\mathbb{C})$-character variety, denoted X_M, using (18). We call X_M^{Fr} the twisted character variety of M. It is more natural than X_M in our setup. See Section 4.1.

The skein module of M is generated by framed links in M. Conveniently, framed curves in M represent elements of $\pi_1(\mathrm{Fr}M)$. Indeed, let α be a smooth path with nonvanishing tangent. A normal framing of α is a unit vector field along α which is everywhere orthogonal to the tangent vector of α. The curve α with a normal framing determines a section of $\mathrm{Fr}M$ along α using the tangent vector, the normal vector, and their cross product.

Every element of $\pi_1(\mathrm{Fr}M)$ can be represented by such a path in M with a normal framing. To do so, first ignore the framing and find a smooth path with the specified tangent vectors at the endpoints. If we assign a random normal framing, it is either homotopic to the given element in $\pi_1(\mathrm{Fr}M)$ or differ by a full rotation in the fiber. The latter can be inserted in the normal framing.

3.2. **Cell decomposition.** Given a triangulation $\mathcal{T}$, we define a cell decomposition (a CW complex) on M that is convenient to use in the frame bundle $\mathrm{Fr}M$.

Take the dual surface $\mathcal{H}_{\mathcal{T}} := (\Sigma_{\mathcal{T}}, \{A_f\}, \{B_e\})$. For technical reasons involving orientations and smoothness, we replace each A_f and B_e with two parallel copies. If we cut along all parallels of A_f, we get annuli between the parallels and lanterns in each tetrahedron, and each lantern is decorated with two parallels for every standard arc. These parallels define a cell structure on $\Sigma_{\mathcal{T}}$, which is extended to a cell structure on M by attaching 2-cells along all parallels of A-curves and B-curves, and then filling in with 3-cells inside the cylinders bounded by parallel curves and inside the lanterns. We can simplify this cell structure by contracting the transverse edges between parallel A-curves. Let $\mathfrak{T}$ denote the cell structure of M after the contraction.

If we also collapse the cylinders bounded by parallel A-curves in the transverse direction, or equivalently, if we do not double the A-curves, we obtain the cell structure in [GGZ15] using doubly truncated tetrahedra. Here, a doubly truncated tetrahedron is obtained from an ideal tetrahedron by truncating the vertices and then the edges. See Figure 5. Then M decomposes as the union of the double truncation of all tetrahedra and the prism neighborhoods of the edges. See the same figure for an example of an edge with valence 4.

Following [GGZ15], the 1-skeleton of the doubly truncated cell structure consists of three types of edges, namely short, medium and long, denoted by γ, β and α, respectively. The

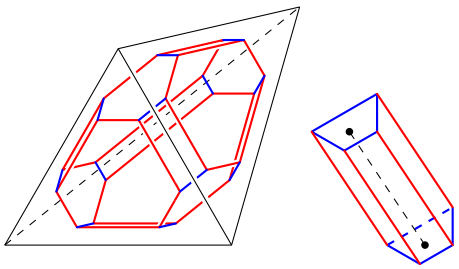

FIGURE 5. Doubly truncated tetrahedron and prism neighborhood of an edge.

short edges are arcs on the parallels of the B-curves. The edges on the A-curves are divided into two types. The long ones are parallel to the edges of the tetrahedra and the rest are the medium ones. In [GGZ15] there is a systematic way to label different edges in each tetrahedron, but we will not need it here.

To connect with the frame bundle $\mathrm{Fr}M$, we need a smooth version of the 1-skeleton. By construction, the 1-skeleton can be drawn on $\Sigma_{\mathcal{T}}$. The γ edges are already joined smoothly since they are segments of B-curves. For the α and β edges, we homotope them according to Figure 6, where orientations are also chosen for the edges. The key here is that at each point of the 0-skeleton, the tangent vectors of the edges all agree.

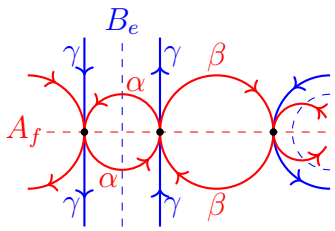

FIGURE 6. A smooth 1-skeleton of $\mathfrak{T}$ on $\Sigma_{\mathcal{T}}$.

Now we also describe the 2-cells of $\mathfrak{T}$. From Figure 6, we can see the disks bounded by α^2 and β^2, which come from the doubling of A-curves. The rest of the 2-cells can be seen in Figure 5. Two types are on the surface $\Sigma_{\mathcal{T}}$ and partially visible in Figure 6: the hexagons $(\gamma^{-1}\beta)^3$ near the vertices of the tetrahedra and the rectangles $(\alpha^{-1}\gamma)^2$ near the edges of the tetrahedra. Finally, two more types are not on $\Sigma_{\mathcal{T}}$: the hexagons $(\alpha^{-1}\beta)^3$ near the faces and the polygons γ^n at the bases of the edge prisms. Here, the boundaries of the 2-cells are expressed as a concatenation of edges. We did not distinguish between different edges of the same type, but the notation makes sense since at each point of the 0-skeleton, the labels α, β, γ and their inverses uniquely determine the next edge.

By the construction of the last section, each edge of the 1-skeleton $\mathfrak{T}^{(1)}$ determines a path in $\mathrm{Fr}M$. The condition on the tangent vectors at the 0-skeleton implies that these paths glue together to define a section $s : \mathfrak{T}^{(1)} \to \mathrm{Fr}M$.

The section s cannot be extended to the entire 2-skeleton by the following lemma, but it is a natural construction, and it allows us to define representations in Proposition 3.3 without making additional choices.

Lemma 3.1. The section s extends over the 2-cells bounded by the hexagons $(\alpha^{-1}\beta)^3$ and $(\gamma^{-1}\beta)^3$. s does not extend over 2-cells bounded by the circles α^2, β^2, the rectangles $(\alpha^{-1}\gamma)^2$, or the polygons around the edges γ^n.

Proof. First we consider the 2-cells on the surface $\Sigma_{\mathcal{T}}$, which are α^2, β^2, $(\alpha^{-1}\gamma)^2$, and $(\gamma^{-1}\beta)^3$. To determine if the boundary of such a 2-cell is trivial in $\pi_1(\mathrm{Fr}M)$, we count how many times the tangent vector turns on the surface. α^2 and β^2 are the easiest: they do a full turn. The others are slightly tricky since some edges are traversed in reverse direction. Note the orientations of the edges are used to define the section s, so even if we go backwards, the tangent vector should be the same. With this in mind, it is easy to see that $(\alpha^{-1}\gamma)^2$ does a full turn, and $(\gamma^{-1}\beta)^3$ does two full turns, so the former is nontrivial, while the latter is trivial in $\pi_1(\mathrm{Fr}M)$.

Next, we look at the polygons around the edges γ^n. The normal framing can be taken to lie on the 2-cell bounded by γ^n pointing inward. Thus, the framing does a full turn, which is nontrivial.

Finally, we look at $(\alpha^{-1}\beta)^3$. It is easier to consider $(\alpha\beta)^3$, which is a smooth curve that also bounds a disk in M, and the normal framing of $(\alpha\beta)^3$ is the outward normal of the boundary of the disk. This shows that $(\alpha\beta)^3$ is homotopic to a full turn. Since α^2 is a full turn and $(\alpha^{-1}\beta)^3$ differs from $(\alpha\beta)^3$ by 3 insertions of α^2, $(\alpha^{-1}\beta)^3$ is trivial in $\pi_1(\mathrm{Fr}M)$. □

Corollary 3.2. The section s induces a surjective homomorphism of the fundamental groupoids $s_* : \pi_1(\mathfrak{T}^{(1)}, \mathfrak{T}^{(0)}) \to \pi_1(\mathrm{Fr}M, s(\mathfrak{T}^{(0)}))$.

Proof. Given a path a in $\mathrm{Fr}M$ with endpoints on $s(\mathfrak{T}^{(0)})$, we can require the projection $p(a)$ on M is on the 1-skeleton $\mathfrak{T}^{(1)}$ after a homotopy. Then in $\pi_1(\mathrm{Fr}M, s(\mathfrak{T}^{(0)}))$, a and $s_*(p(a))$ differ by some rotation in the fiber, which is in the image of s_*. Thus, every element a is in the image of s_*. □

3.3. **Representations.** In this section we discuss how to assign $\mathrm{SL}_2(\mathbb{C})$-representations to points of the gluing equations variety $G_{\mathcal{T}}$. Since the γ edges goes around the edges of the tetrahedra, each γ edge is assigned a shape parameter z_γ.

Proposition 3.3. Given a point $z \in G_{\mathcal{T}}$, the assignment of matrices

$$\alpha \mapsto \begin{pmatrix} 0 & 1 \\ -1 & 0 \end{pmatrix}, \qquad \beta \mapsto \begin{pmatrix} \mathbf{i} & 0 \\ 1 & -\mathbf{i} \end{pmatrix}, \qquad \gamma \mapsto \begin{pmatrix} z_\gamma^{-1} & 0 \\ 0 & z_\gamma \end{pmatrix} \tag{19}$$

to the 1-skeleton $\mathfrak{T}^{(1)}$ defines a homomorphism

$$\pi_1(\mathrm{Fr}M, s(\mathfrak{T}^{(0)})) \to \mathrm{SL}_2(\mathbb{C}). \tag{20}$$

This representation is a lift of the $\mathrm{PGL}_2(\mathbb{C})$-representation given in [GGZ15].

Proof. By comparing (19) with Example 10.15 of [GGZ15], we see that they are conjugate up to scalars. Note our γ has the opposite orientation as their γ^{012}. This implies the lifting property assuming the $\mathrm{SL}_2(\mathbb{C})$-representation here is well-defined.

Let $\rho_s : \pi_1(\mathfrak{T}^{(1)}, \mathfrak{T}^{(0)}) \to \mathrm{SL}_2(\mathbb{C})$ denote the assignment of the matrices. To show that the representation is well-defined, we first look at the images of boundaries of the 2-cells under ρ_s. By a direct calculation, we see that the boundary of a 2-cell maps to I if s extends over the 2-cell or to $-I$ if s does not extend.

Choose a spin structure of M, represented by a section $t : \mathfrak{T}^{(1)} \to \mathrm{Fr}M$ that extends to a section $\bar{t} : M \to \mathrm{Fr}M$. We can require that t agrees with s on $\mathfrak{T}^{(0)}$. Then t determines an embedding $\pi_1(M, \mathfrak{T}^{(0)}) \to \pi_1(\mathrm{Fr}M, s(\mathfrak{T}^{(0)}))$, which is part of an isomorphism

$$\pi_1(M, \mathfrak{T}^{(0)}) \times \mathbb{Z}/2 \xrightarrow[\cong]{\bar{t}_* \cdot i_*} \pi_1(\mathrm{Fr}M, s(\mathfrak{T}^{(0)})). \tag{21}$$

The difference between s_* and t_* is given by a map $e : \pi_1(\mathfrak{T}^{(1)}, \mathfrak{T}^{(0)}) \to \mathbb{Z}/2$. Let $\rho_t : \pi_1(\mathfrak{T}^{(1)}, \mathfrak{T}^{(0)}) \to \mathrm{SL}_2(\mathbb{C})$ be the assignment of matrices modified from ρ_s using the signs determined by e. By construction, ρ_t maps the boundaries of all 2-cells to I. Thus, ρ_t determines a representation $\bar{\rho}_t : \pi_1(M, \mathfrak{T}^{(0)}) \to \mathrm{SL}_2(\mathbb{C})$, which can be extended to

$$\rho : \pi_1(\mathrm{Fr}M, s(\mathfrak{T}^{(0)})) \cong \pi_1(M, \mathfrak{T}^{(0)}) \times \mathbb{Z}/2 \xrightarrow{\bar{\rho}_t \cdot i_*} \mathrm{SL}_2(\mathbb{C}). \tag{22}$$

Then ρ is also the representation induced by ρ_s. To see this, note that $\rho \circ t_* = \rho_t$ by construction. Since t_* and ρ_t are both related to their s-counterparts by e, we get $\rho \circ s_* = \rho_s$. □

Remark 3.4. Recall $Z_j^{\square} = (z_j^{\square})^2$ is the usual shape parameter. Although opposite edges of a tetrahedron have the same shape parameters, they do not need to have the same square roots. For the proof to work, $z_j z_j' z_j'' = \mathbf{i}$ in (5) can be replaced by 4 equations of the same form for triples of edges sharing a vertex in each tetrahedron. These equations imply that $(z_j^{\square})^2$ is the same for opposite edges, but in each tetrahedron, we can choose all 3 pairs of opposite edges to take the same or the opposite square roots.

This is also reflected in the quantization. See Remark 5.1.

4. Skein modules

4.1. **Kauffman bracket skein modules.** In this section we recall the basics of the skein module of a 3-manifold in several flavors. The *skein module* $\mathcal{S}_q(M; R)$ of an oriented 3-manifold M is the R-module generated by the set of isotopy classes of framed unoriented links in M, modulo the relations (1) and (2).

When $M = \Sigma \times (-1, 1)$ is the thickening of an oriented surface Σ, the skein module $\mathcal{S}(M)$ gains an algebra structure by stacking. This means given two links α, β, isotoped such that $\alpha \subset \Sigma \times (0, 1)$ and $\beta \subset \Sigma \times (-1, 0)$, we define $\alpha\beta = \alpha \cup \beta$. Then the skein algebra $\mathcal{S}(\Sigma)$ is the module $\mathcal{S}(M)$ with this product structure.

In this definition, we fix a ring R that contains an invertible element $q^{1/2}$ and a primitive 4-th root of unity $\mathbf{i}$. The two main examples that we are interested in are the universal case $R = R_{\mathrm{univ}} := \mathbb{Z}[\mathbf{i}][q^{\pm 1/2}]$ and the classical limit $R = \mathbb{C}$ with $q^{1/2} = 1$.

Some statements about the skein module are independent of the choice of R and q. We will omit them if the choice is unimportant. When both are omitted, it is usually sufficient to consider the universal case $R = R_{\mathrm{univ}}$. This follows from the universal coefficient property [Prz99, Proposition 2.2(4)]

$$\mathcal{S}_q(M; R) \otimes_R R' \cong \mathcal{S}_{q'}(M; R') \tag{23}$$

induced by a ring homomorphism $r : R \to R'$ with $q' = r(q)$.

The skein module is a quantization of the character variety in the following sense. When $q = \pm 1$, (1) shows that crossing changes do not affect the corresponding elements in

$\mathcal{S}_{\pm 1}(M;\mathbb{C})$. Thus, only the (framed) homotopy classes of the links matter. This also means that disjoint union defines a commutative algebra structure on $\mathcal{S}_{\pm 1}(M;\mathbb{C})$.

In both cases, $\mathcal{S}_{\pm 1}(M;\mathbb{C})$ is related to the coordinate ring of the character variety. Let c be a closed curve in M. Define the *trace function* $t_c : X_M \to \mathbb{C}$ by $t_c(\rho) = \mathrm{tr}(\rho(c))$ for every $\rho : \pi_1(M) \to \mathrm{SL}_2(\mathbb{C})$. It is easy to see that t_c only depends on the conjugacy class of ρ and homotopy class of c, and it is independent of the orientation of c.

Theorem 4.1 ([Bul97])**.** *The algebra homomorphism $\mathcal{S}_{-1}(M;\mathbb{C}) \to \mathbb{C}[X_M]$ sending each knot K to $-t_K$ is surjective, and the kernel is the nilradical of $\mathcal{S}_{-1}(M;\mathbb{C})$.*

This result is not sufficient for our purposes, since the specialization to $q = -1$ is generally not a commutative limit for a quantum torus. It turns out that the specialization to $q = 1$ is related to the twisted character variety X_M^{Fr}. Trace functions can be defined on X_M^{Fr} similarly for smooth curves in M with normal framing.

Lemma 4.2. The algebra homomorphism $\mathcal{S}_1(M;\mathbb{C}) \to \mathbb{C}[X_M^{\mathrm{Fr}}]$ sending each framed knot K to t_K is surjective, and the kernel is the nilradical of $\mathcal{S}_1(M;\mathbb{C})$.

Proof. Fix a spin structure of M. Given a framed knot K, define $\sigma(K) = 1$ if the trivialization of $\mathrm{Fr}M|_K$ determined by the normal framing agrees with the spin structure up to homotopy, and define $\sigma(K) = -1$ otherwise. [Bar99] shows that $K \mapsto -\sigma(K)K$ defines an algebra isomorphism between $\mathcal{S}_{\pm 1}(M;\mathbb{C})$ (in either direction). Similarly, by unpacking the isomorphism $X_M \cong X_M^{\mathrm{Fr}}$ induced by (18), the isomorphism $\mathbb{C}[X_M^{\mathrm{Fr}}] \to \mathbb{C}[X_M]$ of coordinate rings is given by $t_K \mapsto \sigma(K)t_K$ for any framed knot K. Then the corollary follows from Theorem 4.1 combined with these isomorphisms. □

The skein module of a 3-manifold does not change when 3-handles are attached to the manifold, and changes in a predictable way when 2-handles are attached. Indeed, consider the 3-manifold N obtained from M with a 2-handle attached along a smooth curve c on ∂M. c comes with two isotopic normal framings given by the outward and inward normal vectors of ∂M. Let $L \subset M$ be a framed link with a segment close to c where the framing of L and c are opposite. Then there is a well-defined connected sum $L\#c$ which is isotopic to L in N. The operation $L \to L\#c$ in M is called a *handle slide*.

Proposition 4.3 ([Prz99, Proposition 2.2])**.** The inclusion $i : M \hookrightarrow N$ induces a surjective map $i_* : \mathcal{S}(M) \twoheadrightarrow \mathcal{S}(N)$. The kernel is the submodule generated by handle slides.

Remark 4.4. The proof of the proposition does not depend on the details of the defining relations. It only requires the fact that the defining relations of $\mathcal{S}(N)$ can always be performed in M. For the variations of skein modules defined below, we also have handle slides for attaching 2-handles. The proof will be omitted.

Remark 4.5. Although we will not use it in our paper, we remark that the assignement of every framed link in M to its homology class with coefficients in $\mathbb{Z}/2\mathbb{Z}$ induces a $H_1(M, \mathbb{Z}/2\mathbb{Z})$-grading on the skein module $\mathcal{S}(M)$. The quantum trace map preserves that grading.

4.2. **Stated skein modules.** Motivated by the ideas of TQFT, we want a local version of the skein module. This means cutting a 3-manifold along an embedded surface, and doing so, a framed link becomes a framed tangle in the cut manifold. In addition, we will use a

choice of $\pm$ at each boundary point of the framed tangle, thus arriving at the stated framed tangles that we now discuss in detail.

We recall the stated skein modules defined by Lê [LÎ18]. A *punctured bordered surface* is a surface of the form $\Sigma = \overline{\Sigma} \backslash \mathcal{P}$, where $\overline{\Sigma}$ is a compact oriented surface, possibly with boundary and $\mathcal{P}$ is a finite set that intersects every component of $\partial\overline{\Sigma}$. A component of $\partial\Sigma$ is called a *boundary edge*, which is homeomorphic to an open interval. Although the orientation of the surface induces one on its boundary, we will not use the orientation of the boundary at all.

A tangle over Σ is an unoriented embedded 1-dimensional submanifold $\alpha \subset \Sigma \times (-1,1)$ such that

(1) the projection of $\partial\alpha$ is in $\partial\Sigma$, and that
(2) the heights of $\partial\alpha$ (i.e., the image of $\partial\alpha$ under the projection map $\Sigma \times (-1,1) \to (-1,1)$) are distinct over each boundary edge.

A vector $\Sigma \times (-1,1)$ is *vertical* if it is tangent to $\{p\} \times (-1,1)$ in the positive direction. A *framing* of a tangle α over Σ is a transverse vector field along α which is vertical at $\partial\alpha$. A *state* of a tangle α is a map $\partial\alpha \to \{+,-\}$. By convention, $\pm$ are identified with ± 1 when necessary.

Throughout the paper, all tangles will be framed and stated. An *isotopy* of tangles over Σ is homotopy within the class of tangles over Σ. In particular, the height order of $\partial\alpha$ over each boundary edge of Σ is preserved by isotopy.

As usual, tangles are represented by their diagrams. The framing of a diagram is always vertical. At each endpoint, the state is labeled by a sign $\pm$. It is also important to indicate height orders in the diagrams. In the figures drawn below, we use an arrow on the boundary of the surface to indicate that as one follows the direction of the arrow, the heights of the endpoints are consecutive and increasing. This arrow should not be confused with the orientation of the boundary inherited from the orientation of the surface.

Fix a ring R and $q \in R$ as in the introduction. The *stated skein module* $\mathcal{S}_q(\Sigma; R)$ of Σ (abbreviated by $\mathcal{S}(\Sigma)$ when R and q are clear as before) is the R-module spanned by isotopy classes of (framed, stated) tangles over Σ modulo the skein relation (1), the trivial loop relation (2), the trivial arc relations (24), and the state exchange relation (25).

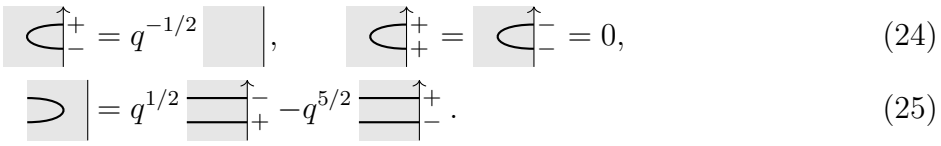

(24)

(25)

In these diagrams, the shaded region is a part of the surface, and the thin line on the side is part of the boundary of the surface.

Remark 4.6. The trivial arc relations (24) as well as (26) below appeared in [BW11]. They are quantizations of the classical matrix entries of the α-matrix as in Equation (89). The powers of q and the relation (25) are required so that splitting in Section 4.5 works, as explained in [LÎ18].

We define additional new quotients of the skein algebra with similar philosophy, where certain arcs are set to scalars that quantize the classical values and make splitting work.

Lemma 4.7 ([LÎ18, Lemmas 2.3 and 2.4])**.** Relations (24) and (25) imply the following.

(1) Trivial arc relation.

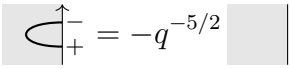

(26)

(2) Height exchange relations.

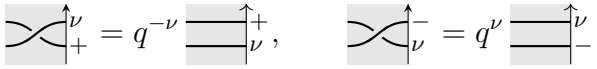

(27)

for $\nu = \pm$.

A tangle diagram is *simple* if it does not have crossings, trivial arcs, or trivial loops. Let $\mathfrak{o}$ be an orientation of $\partial\Sigma$. A diagram is $\mathfrak{o}$-*ordered* if the height over each boundary edge is increasing as one follows $\mathfrak{o}$. All diagrams so far have been positively ordered, meaning $\mathfrak{o}$ is the positive orientation induced by Σ. Finally, a diagram D is *increasingly stated* if there are no endpoints on the same boundary edge such that the higher endpoint has $-$ state and the lower endpoint has $+$ state.

Theorem 4.8 ([LÎ18, Theorem 2.11])**.** *$\mathcal{S}(\Sigma)$ is a free R-module. For any orientation $\mathfrak{o}$, the set of $\mathfrak{o}$-ordered, increasingly stated, simple diagrams is a basis of $\mathcal{S}(\Sigma)$.*

Just as in the case of closed surfaces, the stated skein module $\mathcal{S}(\Sigma)$ has an associative (in general, non-commutative) product given by stacking. Specifically, given tangles $\alpha, \beta \in \mathcal{S}(\Sigma)$, the product $\alpha \cup \beta$ is defined as stacking α above β. What's more, it has a $\mathbb{Z}$-grading associated to each boundary edge e of Σ, defined as follows. For a tangle α with state $s : \partial\alpha \to \{\pm\}$, define

$$d_e(\alpha) = \sum_{x \in \alpha \cap e} s(x) \in \mathbb{Z}\,. \tag{28}$$

It is easy to see that d_e preserves the defining relations (1) and (2), hence it becomes a $\mathbb{Z}$-grading on $\mathcal{S}(\Sigma)$ that is also compatible with the product $\cup$.

Now we consider the reduced skein algebra $\mathcal{S}^{\mathrm{rd}}(\Sigma)$ defined in [CL22]. It is the quotient of $\mathcal{S}(\Sigma)$ by the (two-sided) ideal generated by the *bad arcs*.

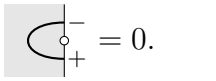

(29)

This relation holds for all possible heights on the boundaries of bad arcs. Same as Remark 4.6, the motivation for this relation is the vanishing entry in the β matrix given in Equation (90).

By [LY22, Corollary 4.6], the left, right, and two-sided ideal generated by the bad arcs agree. For consistency with the quotients later, we usually consider the left ideal.

The following useful result is obtained in the proof of [CL22, Theorem 7.1].

Lemma 4.9. In $\mathcal{S}^{\mathrm{rd}}(\Sigma)$, for a positively ordered diagram of the following form, we have

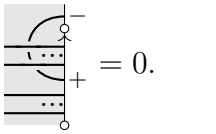

(30)

Theorem 4.10 ([CL22, Theorem 7.1])**.** *$\mathcal{S}^{\mathrm{rd}}(\Sigma)$ is a free R-module. A basis is given by the subset of elements without bad arc components in the basis of $\mathcal{S}(\Sigma)$ from Theorem 4.8 with $\mathfrak{o}$ positive.*

4.3. **Surfaces with triangular boundary.** The closed surface that appears in Proposition 1.2 is obtained by gluing together punctured bordered *surface with triangular boundary*. The latter are punctured bordered surfaces Σ with each boundary component of $\overline{\Sigma}$ containing three boundary edges of Σ. The three boundary edges on the same component of $\partial\overline{\Sigma}$ form a *boundary triangle*. Note that punctures in the interior of $\overline{\Sigma}$ are allowed.

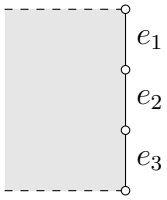

FIGURE 7. Labeling boundary edges in a boundary triangle using the cyclic order induced by the orientation of the boundary triangle.

For a surface Σ with triangular boundary, we need a different product structure on $\mathcal{S}(\Sigma)$, which we denote by $\cdot$. It is modified from $\cup$ by a power of q. The reason for this modification is to obtain the correct quantization (64). See also Section 4.8. Without stating otherwise, we use $\cdot$ as the product for the rest of the paper.

Let $b : \mathbb{Z}^3 \otimes \mathbb{Z}^3 \to \mathbb{Z}$ be the unique skew-symmetric bilinear form that is invariant under cyclic permutations of the components of $\mathbb{Z}^3$ such that $b((1,0,0),(0,1,0)) = 1$. For each boundary triangle $E = \{e_1, e_2, e_3\}$, label the edges as Figure 7. Then the gradings of a tangle α form a vector $d_E(\alpha) = (d_{e_1}(\alpha), d_{e_2}(\alpha), d_{e_3}(\alpha)) \in \mathbb{Z}^3$. For tangles α, β, define a new product by

$$\alpha \cdot \beta = q^{-\frac{1}{2}\sum_E b(d_E(\alpha), d_E(\beta))} \alpha \cup \beta \tag{31}$$

where the sum is over all boundary triangles E. It is easy to see that this extends linearly to an associative product with the empty tangle as unit.

4.4. **Corner-reduced skein module.** In this section Σ denotes a surface with triangular boundary. Let $\mathcal{S}^{\mathrm{cr}}(\Sigma)$ be the quotient of the reduced skein algebra $\mathcal{S}^{\mathrm{rd}}(\Sigma)$ by the left ideal (under $\cdot$ product) generated by the following relations near marked points.

(32)

As mentioned in Remark 4.6, the motivation for these relations are the three nonzero entries of the β-matrix given in Equation (90). Keep in mind that as in (29) the heights in the above relations are arbitrary. Note also that the boundary of the above arcs lies in different boundary edges since the boundary of the above pictures is part of a triangle. By [CL22, Proposition 7.4], the first two are equivalent in $\mathcal{S}^{\mathrm{rd}}(\Sigma)$.

Remark 4.11. Because we do not specify which 4-th root of unity $\mathbf{i}$ is, technically $\mathcal{S}^{\mathrm{cr}}(\Sigma)$ depends on this choice as well, and it is independent of the choice of q. In this paper, the only time this is relevant is in Section 5.4, where we discuss roots of unity.

Lemma 4.12. In $\mathcal{S}^{\mathrm{cr}}(\Sigma)$, the lowest endpoint on a boundary edge can be modified in the following way.

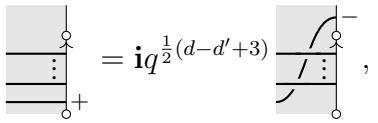

(33)

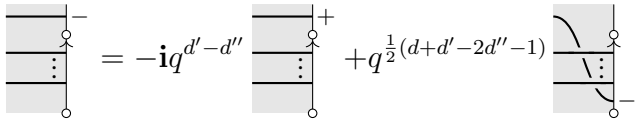

(34)

Here, d and d' are the gradings of the left-hand sides on the top and bottom edges, respectively, and d'' is the grading on the third edge in the same boundary triangle (not shown in the diagrams).

Proof. Let α denote the left-hand side of (33). First we use the definition of the product to combine the diagrams. Then we resolve the lowest crossing.

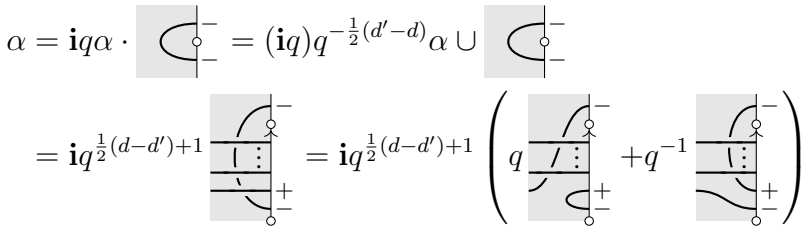

The second term is zero by Lemma 4.9. The first term simplifies to (33).

For (34), still let α denote the left-hand side. Then

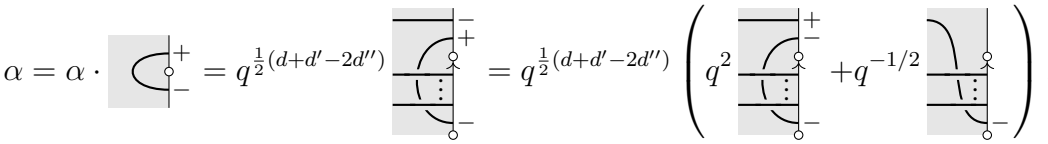

The second term is in the desired form. The first term is a $\cup$-product. By rewriting in terms of the new product, we obtain (34). □

In Lemma 4.12, there are strands unchanged by the relations. They are always higher than the strands changed by the relations, which is the result of the quotient by a left ideal. We will say such relations in $\mathcal{S}^{\mathrm{cr}}(\Sigma)$ holds at the bottom and omit the unchanged strands. By rewriting the relations in the lemma, we obtain the following.

Corollary 4.13. In $\mathcal{S}^{\mathrm{cr}}(\Sigma)$, the following relations hold at the bottom.

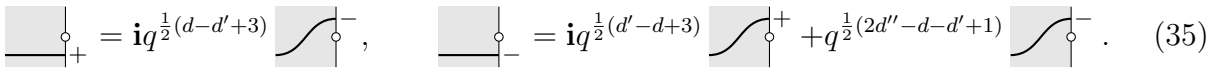

(35)

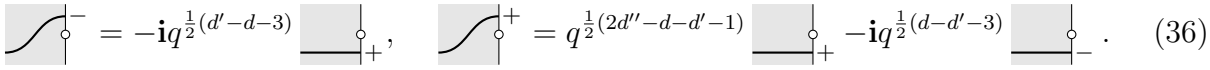

(36)

Here, d, d', d'' have the same meaning as in Lemma 4.12.

Note that these moves do not preserve the gradings d and d'. Although (35) and (36) are inverses, a naive substitution does not show this, because the gradings need to be adjusted.

Lemma 4.14. Suppose Σ is a surface with triangular boundary. In $\mathcal{S}^{\mathrm{cr}}(\Sigma)$, the following handle slide moves hold at the bottom.

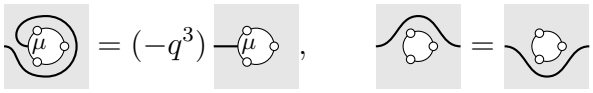

(37)

Proof. The first identity is obtained by applying (35) three times. For the second one, we redraw it as

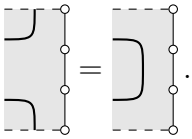

(38)

To prove this, we combine the first identity with (25).

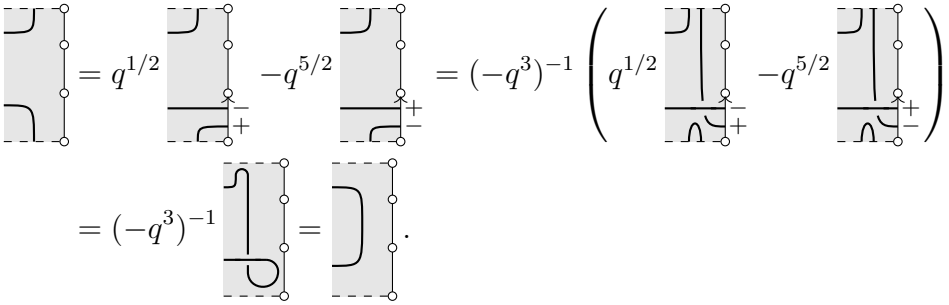

□

4.5. **Splitting.** The stated skein algebra and its reduced version have splitting homomorphisms connecting the punctured bordered surfaces before and after splitting, thus reducing the surfaces to elementary pieces, namely a standard monogon, bigon, and triangle shown in Figure 8. We briefly recall how this works.

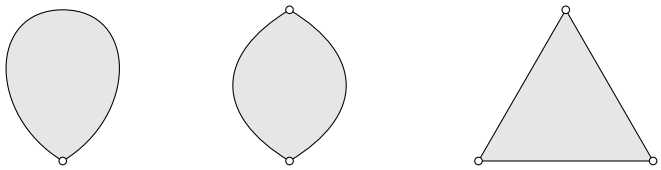

FIGURE 8. Elementary surfaces: monogon, bigon, and triangle.

Let $\Sigma = \overline{\Sigma} \setminus \mathcal{P}$ be a punctured bordered surface. An *ideal arc* on Σ is a simple arc $e : [0,1] \to \overline{\Sigma}$ such that $e(0), e(1) \in \mathcal{P}$ and $e((0,1))$ is in the interior of Σ. Splitting Σ along e produces a new punctured bordered surface denoted Σ_e. There is a quotient map $p : \Sigma_e \to \Sigma$ gluing the new boundary edges back. Let $\widetilde{p} : \Sigma_e \times (-1,1) \to \Sigma \times (-1,1)$ be the induced map.

Fix an ideal arc e on a punctured bordered surface Σ, and a tangle α over Σ. Isotope α such that it is transverse to $\widetilde{e} = e \times (-1,1)$ and the heights of $\alpha \cap \widetilde{e}$ are distinct, and define

$$\Theta_e(\alpha) = \sum_{s : \alpha \cap \widetilde{e} \to \{\pm\}} (\alpha, s), \tag{39}$$

where (α, s) is the tangle $\widetilde{p}^{-1}(\alpha)$ with the state $s(x)$ assigned to both points in $\widetilde{p}^{-1}(x)$ for all $x \in \alpha \cap \widetilde{e}$.

Theorem 4.15 ([Lî18, Theorem 3.1], [CL22, Thm. 7.6]). *Given an ideal arc e on a punctured bordered surface Σ, (39) is a well-defined algebra homomorphism (with respect to $\cup$)*

$$\Theta_e : \mathcal{S}(\Sigma) \to \mathcal{S}(\Sigma_e) \tag{40}$$

that satisfies

$$\Theta_e \circ \Theta_f = \Theta_f \circ \Theta_e \tag{41}$$

if e and f are disjoint ideal arcs in Σ, and descends to an algebra homomorphism

$$\Theta_e : \mathcal{S}^{\mathrm{rd}}(\Sigma) \to \mathcal{S}^{\mathrm{rd}}(\Sigma_e), \tag{42}$$

denoted by Θ_e by abuse of notation.

Now suppose $\Sigma = \overline{\Sigma} \setminus \mathcal{P}$ has triangular boundary. When we consider the corner reduced skein module $\mathcal{S}^{\mathrm{cr}}(\Sigma)$, we can split along a closed curve c in the interior of Σ with three distinguished points $p_1, p_2, p_3 \in c$. Let $\Sigma'_c = \Sigma \setminus \{p_1, p_2, p_3\}$. Then $c \cap \Sigma'_c$ is the union of three ideal arcs in Σ'_c. Σ'_c split along these arcs is a surface Σ_c with triangular boundary. Let $\Theta : \mathcal{S}(\Sigma'_c) \to \mathcal{S}(\Sigma_c)$ be the composition of splits.

Theorem 4.16. *The composition of splits $\Theta : \mathcal{S}(\Sigma'_c) \to \mathcal{S}(\Sigma_c)$ induces an R-module homomorphism $\Theta_c : \mathcal{S}^{\mathrm{cr}}(\Sigma) \to \mathcal{S}^{\mathrm{cr}}(\Sigma_c)$.*

$$\begin{array}{ccc} \mathcal{S}(\Sigma'_c) & \xrightarrow{\Theta} & \mathcal{S}(\Sigma_c) \\ \downarrow\!\!\downarrow & & \\ \mathcal{S}(\Sigma) & & \downarrow\!\!\downarrow \\ \downarrow\!\!\downarrow & & \\ \mathcal{S}^{\mathrm{cr}}(\Sigma) & \xrightarrow{\Theta_c} & \mathcal{S}^{\mathrm{cr}}(\Sigma_c) \end{array} \tag{43}$$

Proof. First consider the descent to $\mathcal{S}(\Sigma) \to \mathcal{S}^{\mathrm{cr}}(\Sigma_c)$. The map $\mathcal{S}(\Sigma'_c) \twoheadrightarrow \mathcal{S}(\Sigma)$ is induced by the inclusion $\Sigma'_c \hookrightarrow \Sigma$. The kernel of this quotient is generated by isotopies across the punctures p_1, p_2, p_3, or in terms of diagrams,

(44)

We need to show that the splitting of both sides are equal in $\mathcal{S}^{\mathrm{cr}}(\Sigma_c)$. We can always isotope the tangle such that the intersection with $\tilde{c} = c \times (-1, 1)$ is the lowest. Thus, we only need to check the equality at the bottom.

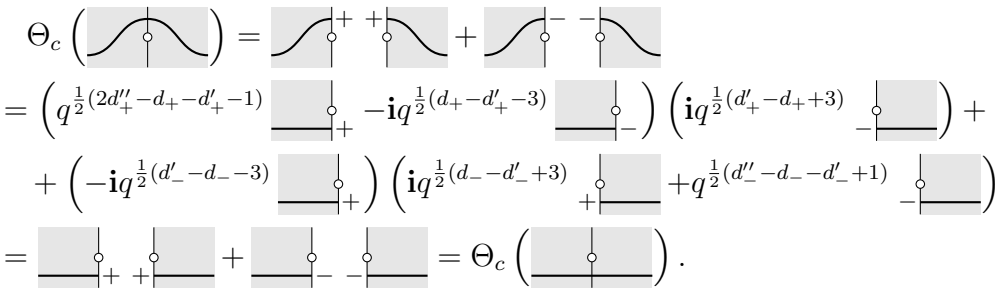

Here, Corollary 4.13 is applied to every factor, where $d_\pm, d'_\pm, d''_\pm$ are the gradings of 

. Then $d_+ = d_- + 2$ and $d'_+ = d'_-, d''_+ = d''_-$. Note for 

, a rotation is necessary for

Corollary 4.13 to apply, which is why the primes do not match. Note in the right half of each term, the direction of twist is opposite of the left half because of the orientation. This shows $\mathcal{S}(\Sigma) \to \mathcal{S}^{\mathrm{cr}}(\Sigma_c)$ is well-defined.

The descent to $\Theta_c : \mathcal{S}^{\mathrm{cr}}(\Sigma) \to \mathcal{S}^{\mathrm{cr}}(\Sigma_c)$ is trivial. The splitting homomorphism only affects a neighborhood of c, whereas the quotient $\mathcal{S}(\Sigma) \twoheadrightarrow \mathcal{S}^{\mathrm{cr}}(\Sigma)$ happens near $\partial\Sigma$. □

If the split surface $\Sigma_c = \Sigma_1 \sqcup \Sigma_2$ is disconnected, then $\mathcal{S}^{\mathrm{cr}}(\Sigma_c)$ is naturally isomorphic to $\mathcal{S}^{\mathrm{cr}}(\Sigma_1) \otimes \mathcal{S}^{\mathrm{cr}}(\Sigma_2)$. In this case, the splitting homomorphism has the form

$$\Theta_c : \mathcal{S}^{\mathrm{cr}}(\Sigma) \to \mathcal{S}^{\mathrm{cr}}(\Sigma_1) \otimes \mathcal{S}^{\mathrm{cr}}(\Sigma_2). \tag{45}$$

4.6. **The skein of the bigon and action of $\mathcal{O}_{q^2}(\mathrm{SL}_2)$.** The splitting Theorem 4.15 of the previous section reduces the study of the stated skein module of a surface to that of an elementary surface. In this and in the next sections we study three examples of elementary punctured bordered surfaces, namely the standard bigon, annulus and the lantern.

We begin with the bigon $\mathbb{B}$ shown in Figure 9. It contains the tangle $a_{\mu\nu}$ with states μ, ν at $a(0), a(1)$ respectively.

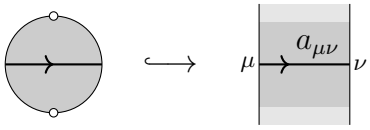

FIGURE 9. Bigon neighborhood of an arc.

The skein module $\mathcal{S}(\mathbb{B})$ of the bigon can be identified with the quantum matrix group $\mathcal{O}_{q^2}(\mathrm{SL}_2)$ generated by a, b, c, d with relations

$$\begin{aligned} &ca = q^2 ac, \qquad db = q^2 bd, \qquad ba = q^2 ab, \qquad dc = q^2 cd \\ &bc = cb, \qquad ad - q^{-2} bc = 1, \qquad da - q^2 cb = 1\,. \end{aligned} \tag{46}$$

See [Maj95] and also [CL22, Defn. 1]. Explicitly, in [CL22, Theorem 3.4], it was shown that there is an isomorphism

$$\mathcal{O}_{q^2}(\mathrm{SL}_2) \to \mathcal{S}(\mathbb{B}) \tag{47}$$

given by mapping a, b, c, d of $\mathcal{O}_{q^2}(\mathrm{SL}_2)$ to a_{++}, a_{+-}, a_{-+} and a_{--}, and checking that the defining relations (46) hold true.

The skein of a bigon acts on the skein of a punctured bordered surface Σ as follows. Fix an oriented simple arc $a : [0,1] \to \Sigma$ whose endpoints are on different boundary triangles of Σ. The inclusion of the bigon induces an R-module embedding

$$\phi_a : \mathcal{O}_{q^2}(\mathrm{SL}_2) \hookrightarrow \mathcal{S}(\Sigma)\,. \tag{48}$$

By the assumption that a ends on distinct boundary triangles, the factor in (31) is trivial. Therefore, the two product structures match. Since $\mathcal{S}^{\mathrm{cr}}(\Sigma)$ is a left $\mathcal{S}(\Sigma)$-module, it induces a left $\mathcal{O}_{q^2}(\mathrm{SL}_2)$-module structure.

This module structure is compatible with splitting in the following sense. Suppose c is a simple closed curve in the interior of Σ that intersects the arc a once transversely. Let

a', a'' be the arcs on Σ_c obtained by splitting a at $a \cap c$. Then the arcs a', a'' induces an $(\mathcal{O}_{q^2}(\mathrm{SL}_2) \otimes \mathcal{O}_{q^2}(\mathrm{SL}_2))$-action on $\mathcal{S}^{\mathrm{cr}}(\Sigma_c)$.

Lemma 4.17. The following diagram is commutative

$$\begin{array}{ccc} \mathcal{O}_{q^2}(\mathrm{SL}_2) \otimes \mathcal{S}^{\mathrm{cr}}(\Sigma) & \xrightarrow{\Delta \otimes \Theta_c} & (\mathcal{O}_{q^2}(\mathrm{SL}_2) \otimes \mathcal{O}_{q^2}(\mathrm{SL}_2)) \otimes \mathcal{S}^{\mathrm{cr}}(\Sigma_c) \\ \downarrow & & \downarrow \\ \mathcal{S}^{\mathrm{cr}}(\Sigma) & \xrightarrow{\Theta_c} & \mathcal{S}^{\mathrm{cr}}(\Sigma_c) \end{array} \tag{49}$$

Here, the vertical arrows are the module actions, and Δ is the coproduct of $\mathcal{O}_{q^2}(\mathrm{SL}_2)$.

Proof. This is obvious using the identification of Δ with the unique splitting homomorphism of the bigon, which is proved in [CL22, Theorem 3.4]. □

4.7. **The skein of the annulus.** Fix 3 points $p_1, p_2, p_3 \in S^1$. Then the annulus $S^1 \times [0,1]$ becomes a surface with triangular boundary $\mathbb{A} = (S^1 \times [0,1]) \setminus \mathcal{P}$ where $\mathcal{P} = \{p_1, p_2, p_3\} \times \{0,1\}$. We call $\mathbb{A}$ the *standard annulus*.

If we split $\mathbb{A}$ along its core $S^1 \times 1/2$ and choose the new marked points at $\{p_1, p_2, p_3\} \times 1/2$, then the two components are canonically identified with standard annulus. Then the splitting homomorphism is a comultiplication

$$\Delta : \mathcal{S}^{\mathrm{cr}}(\mathbb{A}) \to \mathcal{S}^{\mathrm{cr}}(\mathbb{A}) \otimes \mathcal{S}^{\mathrm{cr}}(\mathbb{A}). \tag{50}$$

It is coassociative by the commuting property of the splitting homomorphism.

Fix $p \in S^1 \setminus \{p_1, p_2, p_3\}$, and let $a : [0,1] \to \mathbb{A}$, $a(t) = (p, t)$. In the last section, we defined a left $\mathcal{O}_{q^2}(\mathrm{SL}_2)$-action on $\mathcal{S}^{\mathrm{cr}}(\mathbb{A})$ along a. By Lemma 4.17, the action is compatible with the comultiplication. Thus, $\mathcal{S}^{\mathrm{cr}}(\mathbb{A})$ is a left $\mathcal{O}_{q^2}(\mathrm{SL}_2)$-module-coalgebra.

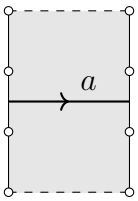

FIGURE 10. Standard annulus.

Theorem 4.18. *The action of $\mathcal{O}_{q^2}(\mathrm{SL}_2)$ on the empty diagram defines an isomorphism of left $\mathcal{O}_{q^2}(\mathrm{SL}_2)$-module-coalgebras.*

$$\phi_a : \mathcal{O}_{q^2}(\mathrm{SL}_2) \to \mathcal{S}^{\mathrm{cr}}(\mathbb{A}). \tag{51}$$

The proof is given in Appendix A.

Corollary 4.19. The comultiplication Δ on $\mathcal{S}^{\mathrm{cr}}(\mathbb{A})$ has a counit such that

$$\epsilon(a_{\mu\nu}) = \delta_{\mu\nu}, \tag{52}$$

where $a_{\mu\nu}$ is defined in the last section.

Suppose Σ is a surface with triangular boundary, and c is a simple closed curve parallel to a boundary triangle. Then the splitting homomorphism along c is a $\mathcal{S}^{\mathrm{cr}}(\mathbb{A})$-comodule structure for $\mathcal{S}^{\mathrm{cr}}(\Sigma)$.

Proof. Since $\mathcal{O}_{q^2}(\mathrm{SL}_2)$ has a counit, it can be transferred to $\mathcal{S}^{\mathrm{cr}}(\mathbb{A})$, which gives (52).
The second part is the same as [CL22, Proposition 4.1(a)]. □

Note the isomorphism ϕ_a depends on the choice of the point p that determines the arc a. However, the corollary does not, since the counit ϵ is uniquely determined by the co-multiplication Δ. The isomorphism is used to show that (52) is sufficient to define the counit.

The corollary is very useful for calculation. We give one example which is used later.

Lemma 4.20. In $\mathcal{S}^{\mathrm{cr}}(\Sigma)$, we have

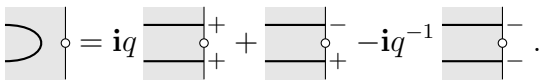

(53)

Here, the left-hand side has no endpoints on the boundary triangle.

Proof. Apply the comodule structure and then the counit.

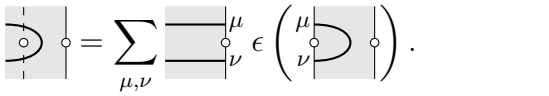

(54)

The tangle in the counit evaluates to scalars by the defining relations of $\mathcal{S}^{\mathrm{cr}}$, including the bad arc relation of $\mathcal{S}^{\mathrm{rd}}$. The lemma is obtained after substitution. □

4.8. **Interlude: basics on the quantum torus.** In this section we include a short discussion on the quantum torus, which is an example of a skew Laurent polynomial ring. For more details, see e.g. [GW89].

Given a skew-symmetric $r \times r$ matrix B with integer entries, the quantum torus $\mathbb{T}(B)$ is defined by

$$\mathbb{T}(B) = R\langle x_1^{\pm 1}, \dots, x_r^{\pm 1}\rangle / \langle x_i x_j - q^{B_{ij}} x_j x_i \rangle. \tag{55}$$

If we use notations other than x_j for the generators and specify the q-commuting relations elsewhere, we simply write the generators as in the introduction.

The quantum torus is an associative, and in general non-commutative algebra with unit. Additively, there is an R-linear isomorphism from the Laurent polynomial ring

$$R[t_1^{\pm 1}, \dots, t_r^{\pm 1}] \xrightarrow{\cong} \mathbb{T}(B). \tag{56}$$

The image of the monomial $t_1^{k_1} \cdots t_r^{k_r}$ is the *Weyl-ordered monomial* in $\mathbb{T}(B)$.

$$x^{\mathbf{k}} = q^{-\frac{1}{2}\sum_{i<j} B_{ij}} x_1^{k_1} \cdots x_r^{k_r}, \qquad \mathbf{k} = (k_1, \dots, k_r) \in \mathbb{Z}^r. \tag{57}$$

These monomial q-commute according to the bilinear form $\langle \cdot, \cdot \rangle_B$ associated to B on $\mathbb{Z}^r$.

$$x^{\mathbf{k}} x^{\mathbf{l}} = q^{\frac{1}{2}\langle \mathbf{k}, \mathbf{l}\rangle_B} x^{\mathbf{k}+\mathbf{l}} = q^{\langle \mathbf{k}, \mathbf{l}\rangle_B} x^{\mathbf{k}} x^{\mathbf{l}}. \tag{58}$$

This normalization can be formally understood as the Baker-Campbell-Hausdorff formula for $e^{\sum_i k_i \ln(x_i)}$.

Note that Weyl-ordering can be defined for all products with q-commuting factors. Weyl-ordering is also related to the product structures on the skein algebra $\mathcal{S}(\Sigma)$ of a surface Σ with triangular boundary. Let α, β be two disjoint diagrams on Σ such that no boundary edge contains endpoint of both α and β. Then by definition, $\alpha \cup \beta$ is commuting, but $\alpha \cdot \beta$ is q-commuting. Comparing Definition (31) with (58), we see that the $\cup$-product is the Weyl-ordering of $\cdot$-product in this case. This observation is used in the next section.

4.9. **The skein of the lantern.** Recall the standard lantern $\mathbb{L}$ defined in Section 2.1. On each boundary component of $\mathbb{L}$, delete a point between each pair of endpoints of standard arcs. This gives a surface with triangular boundary. See Figure 11. We use $\mathbb{L}$ to denote the compact surface except in skein modules where triangular boundaries are required.

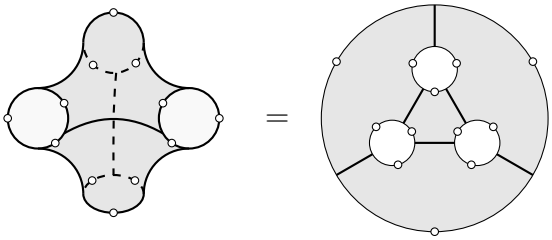

FIGURE 11. The standard lantern with triangular boundary.

Let $\phi^i : \mathcal{O}_{q^2}(\mathrm{SL}_2) \to \mathcal{S}(\mathbb{L})$, $i = 1, \dots, 6$, denote the embedding along the standard arcs a^i. They fit together to define an R-linear map

$$\phi : \mathcal{O}_{q^2}(\mathrm{SL}_2)^{\otimes 6} \to \mathcal{S}(\mathbb{L}), \qquad \phi(x^1 \otimes \cdots \otimes x^6) = \phi^1(x^1) \cup \cdots \cup \phi^6(x^6)\,. \tag{59}$$

Lemma 4.21. ϕ is an algebra embedding if we use the $\cup$-product $\mathcal{S}(\mathbb{L})$. Hence, its $\mathcal{S}^0$ is a subalgebra (for both products).

Proof. ϕ is injective using the basis from Theorem 4.8. Each ϕ_i is an algebra embedding, and their images commute with each other under $\cup$ since the standard arcs all end on different boundary edges. Thus, ϕ is an algebra map if we use the $\cup$-product on $\mathcal{S}(\mathbb{L})$. Then clearly, the image is a subalgebra under $\cup$, but the two products differ by a scalar, so it is also a subalgebra under $\cdot$. □

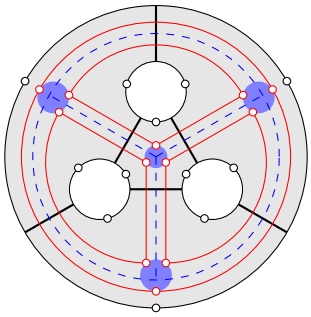

FIGURE 12. Splitting the standard lantern.

Lemma 4.22. The restriction of the quotient $\mathcal{S}(\mathbb{L}) \twoheadrightarrow \mathcal{S}^{\mathrm{cr}}(\mathbb{L})$ to $\mathcal{S}^0$ is surjective.

Proof. We start by drawing a graph dual to the standard arcs. See the dashed blue graph in Figure 12. Given any diagram on $\mathbb{L}$, we can assume that it is disjoint from the vertices of the blue graph and transverse to the edges. Then we draw 4 curves isotopic to the boundary triangles and very close to the graph, and we put punctures on the curves close to the vertices of the graph. See the red curves in the same figure. Now we use the comodule property to split along the red curves and apply the counit to the annuli. The result is the same element in $\mathcal{S}^{\mathrm{cr}}(\mathbb{L})$ but given as a sum of new diagrams. If the red curves are close enough to the graph, then each term is a diagram consisting of standard arcs. Such a diagram is in the image of ϕ. □

Let $\widehat{\mathcal{G}}(\mathbb{L})$ denote the quotient of $\mathcal{S}^{\mathrm{cr}}(\mathbb{L})$ by the left ideal generated by standard arcs with opposite states assigned to the endpoints. In other words, the left ideal is generated by

$$a^i_{+-} = a^i_{-+} = 0, \qquad i = 1, \dots, 6 \tag{60}$$

using the notation of Section 4.6. The motivation for this relation is the vanishing of the off-diagonal entries of the γ matrix given in Equation (91).

Since $\mathcal{S}^{\mathrm{cr}}(\mathbb{L})$ is also a quotient of $\mathcal{S}^0 \subset \mathcal{S}(\mathbb{L})$, we can obtain $\widehat{\mathcal{G}}(\mathbb{L})$ using a different order of quotients. Let $\mathbb{T}^0$ be the quotient of $\mathcal{S}^0$ by (60). We should consider the left ideal in the quotient, but using the definition (46) of $\mathcal{O}_{q^2}(\mathrm{SL}_2)$, it is easy to see that the left ideal is also two-sided. Also from the definition, since we set the off-diagonal elements of $\mathcal{O}_{q^2}(\mathrm{SL}_2)$ to 0, we have

$$\mathbb{T}^0 = R[(a^1_{--})^{\pm 1}, \dots, (a^6_{--})^{\pm 1}] \tag{61}$$

when we use $\cup$ product, which implies that $\mathbb{T}^0$ is a quantum torus under $\cdot$ by the discussion in Section 4.8. Here, inverses are given by $(a^i_{--})^{-1} = a^i_{++}$. This shows $\widehat{\mathcal{G}}(\mathbb{L})$ is a quotient of a quantum torus.

In the next section, we show that the corner reductions for $\mathbb{T}^0$ are equivalent to the Lagrangian equation, which justify the notation $\widehat{\mathcal{G}}(\mathbb{L})$. However, this is not obvious a priori, so we choose to define $\widehat{\mathcal{G}}(\mathbb{L})$ as a quotient of $\mathcal{S}^{\mathrm{cr}}(\mathbb{L})$, which is better for the splitting homomorphism.

Lemma 4.23. The quotient (60) is 2-sided in the sense that

$$a^i_{+-} \cdot \widehat{\mathcal{G}}(\mathbb{L}) = a^i_{-+} \cdot \widehat{\mathcal{G}}(\mathbb{L}) = 0. \tag{62}$$

Proof. This is true for $\mathbb{T}^0$, so it holds for the quotient $\widehat{\mathcal{G}}(\mathbb{L})$. □

4.10. **Presentation of $\widehat{\mathcal{G}}(\mathbb{L})$.** We described $\widehat{\mathcal{G}}(\mathbb{L})$ as some quotient of $\mathbb{T}^0$. In this section we give a presentation for this quotient. To make connection to the quantum gluing module, we rename the standard arcs.

The standard arcs cut $\mathbb{L}$ into 4 components, dual to the ideal vertices. Choose one of these components and one standard arc on it to label as b. Label the other two arcs b', b'' as shown in Figure 13, and label the arc opposite to $b^{\square}$ by $c^{\square}$.

Let

$$\hat{z}^{\square} = b^{\square}_{--}, \ \hat{y} = c^{\square}_{--} \in \mathcal{S}(\mathbb{L}). \tag{63}$$

By the definition of the product (31),

$$\hat{z}''\hat{z} = q\hat{z}\hat{z}'', \qquad \hat{y}\hat{z} = \hat{z}\hat{y}. \tag{64}$$

Other q-commuting relations, e.g. $\hat{z}\hat{y}' = q\hat{y}'\hat{z}$, can be obtained by symmetry. These are also used as the q-commuting relations of $\mathbb{T}^0$.

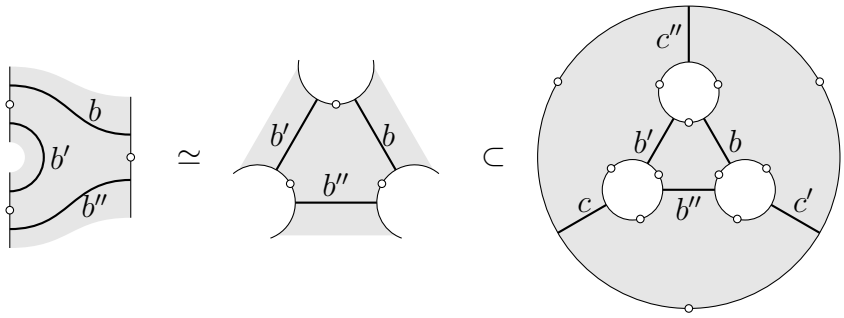

FIGURE 13. Labeling arcs on the standard lantern.

Lemma 4.24. In $\widehat{\mathcal{G}}(\mathbb{L})$, we have

$$\hat{z}\hat{z}'\hat{z}'' = \mathbf{i}q^{3/2}, \qquad \hat{z}^{-2} + (\hat{z}'')^2 = 1\,. \tag{65}$$

Proof. To prove the first identity, start with $\hat{z}' = b'_{--}$ and apply Corollary 4.13.

$$\hat{z}' = \quad = (-\mathbf{i}q^{-1}) \cdot q \left(\mathbf{i} \quad + \quad \right) \tag{66}$$

After applying (53), the diagrams are of the form $b_{\mu\nu} \cup b''_{\mu''\nu''}$. This is zero if $\mu \neq \nu$ or $\mu'' \neq \nu''$. Therefore, the only nonzero term after (53) is

$$\hat{z}' = \mathbf{i}q \quad = \mathbf{i}q\hat{z}^{-1} \cup (\hat{z}'')^{-1}. \tag{67}$$

This is equivalent to $\hat{z}\hat{z}'\hat{z}'' = \mathbf{i}q^{3/2}$.

The second identity is similar, starting with $b'_{+-} = 0$ where the $+$ state is the top endpoint.

$$0 = \quad = \mathbf{i} \quad + \quad + \quad - \mathbf{i} \quad$$

The first two terms are calculated before, and the last two terms are similar. We get

$$= \mathbf{i}(\mathbf{i}q) \quad + 0 + \quad - \mathbf{i}(-\mathbf{i}q^{-1}) \quad$$

$$= -q\hat{z}^{-1} \cup (\hat{z}'')^{-1} + \hat{z} \cup (\hat{z}'')^{-1} - q^{-1}\hat{z} \cup \hat{z}''.$$

After multiplying on the left by $\hat{z}^{-1} \cup \hat{z}''$, we get $\hat{z}^{-2} + (\hat{z}'')^2 = 1$. □

Remark 4.25. The same calculations can be done with b'_{++} and b'_{-+}, but they do not give additional relations.

The next theorem gives a promised presentation for the $\widehat{\mathcal{G}}(\mathbb{L})$ module.

Theorem 4.26. *We have*

$$\widehat{\mathcal{G}}(\mathbb{L}) = \mathbb{T}\langle \hat{z}, \hat{z}'', \hat{y} \rangle /_L \langle \hat{z}^{-2} + (\hat{z}'')^2 - 1, \hat{z}^2 - \hat{y}^2 \rangle \,. \tag{68}$$

Proof. Let $\widehat{\mathcal{G}}^0$ denote the quotient of $\mathbb{T}^0$ by the left ideal generated by (65) as well as the relations obtained by symmetries of $\mathbb{L}$. This includes the vertex equations

$$\hat{z}\hat{z}'\hat{z}'' = \hat{z}\hat{y}'\hat{y}'' = \hat{y}\hat{z}'\hat{y}'' = \hat{y}\hat{y}'\hat{z}'' = \mathbf{i}q^{3/2}. \tag{69}$$

Similarly, there are 12 Lagrangian equations. We can eliminate $\hat{z}', \hat{y}', \hat{y}''$ using the vertex equations. Then we get $\hat{z}^2 = \hat{y}^2$, and only one Lagrangian $\hat{z}^{-2} + (\hat{z}'')^2 = 1$ is required. Thus,

$$\widehat{\mathcal{G}}^0 = \mathbb{T}\langle \hat{z}, \hat{z}'', \hat{y} \rangle /_L \langle \hat{z}^{-2} + (\hat{z}'')^2 - 1, \hat{z}^2 - \hat{y}^2 \rangle. \tag{70}$$

The discussion prior to the theorem shows that there is a surjective map $f : \widehat{\mathcal{G}}^0 \to \widehat{\mathcal{G}}(\mathbb{L})$. Now we find the inverse.

Recall the setup of Lemma 4.22. For each vertex of the blue graph, draw a small disk around it such that the punctures on the red curves are on the boundary of the disk. See the light blue disks in Figure 12. Let $\mathbb{L}'$ be $\mathbb{L}$ minus the closure of the disks. Then the red curves break into 12 ideal arcs on $\mathbb{L}'$.

If we split $\mathbb{L}'$ along the 12 red ideal arcs, then the surface becomes 4 standard annuli and 6 bigons. Thus, the splitting homomorphism has the form $\mathcal{S}(\mathbb{L}') \to (\mathcal{S}(\mathbb{A})^{\otimes 4}) \otimes (\mathcal{S}(\mathbb{B})^{\otimes 6})$. If we consider the corner reduction $\mathcal{S}^{\mathrm{cr}}(\mathbb{L}')$, the defining relations (29) and (32) are contained in the annuli, so if we also reduce the annuli, we get

$$\Theta_{\mathrm{red}} : \mathcal{S}^{\mathrm{cr}}(\mathbb{L}') \to (\mathcal{S}^{\mathrm{cr}}(\mathbb{A})^{\otimes 4}) \otimes (\mathcal{S}(\mathbb{B})^{\otimes 6}). \tag{71}$$

Let $k : \mathcal{S}(\mathbb{B})^{\otimes 6} \xrightarrow[\cong]{\phi} \mathcal{S}^0 \twoheadrightarrow \mathbb{T}^0$ be the quotient map. Now consider the composition

$$\tilde{g} : \mathcal{S}^{\mathrm{cr}}(\mathbb{L}') \xrightarrow{\Theta_{\mathrm{red}}} (\mathcal{S}^{\mathrm{cr}}(\mathbb{A})^{\otimes 4}) \otimes (\mathcal{S}(\mathbb{B})^{\otimes 6}) \xrightarrow{(\epsilon^{\otimes 4}) \otimes k} \mathbb{T}^0 \twoheadrightarrow \widehat{\mathcal{G}}^0. \tag{72}$$

The inclusion $\mathbb{L}' \hookrightarrow \mathbb{L}$ induces a surjective map $\mathcal{S}^{\mathrm{cr}}(\mathbb{L}') \twoheadrightarrow \mathcal{S}^{\mathrm{cr}}(\mathbb{L}) \twoheadrightarrow \widehat{\mathcal{G}}(\mathbb{L})$. We claim that $\tilde{g}$ induces a map $g : \widehat{\mathcal{G}}(\mathbb{L}) \to \widehat{\mathcal{G}}^1$. Then it is easy to check that g is inverse to f, which proves the theorem.

To finish the proof, we show that g is well-defined. For this, we need to consider the kernel $I = \ker(\mathcal{S}^{\mathrm{cr}}(\mathbb{L}') \twoheadrightarrow \widehat{\mathcal{G}}(\mathbb{L}))$, which is a left ideal. By definition, the kernel of $\mathcal{S}^{\mathrm{cr}}(\mathbb{L}) \twoheadrightarrow \widehat{\mathcal{G}}(\mathbb{L})$ is generated by (60), which can be lifted to $\mathcal{S}^{\mathrm{cr}}(\mathbb{L}')$. On the other hand, the kernel of $\mathcal{S}^{\mathrm{cr}}(\mathbb{L}') \twoheadrightarrow \mathcal{S}^{\mathrm{cr}}(\mathbb{L})$ is generated by the handle slides.

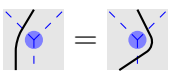 (73)

Together, these relations generate I as a left ideal in $\mathcal{S}^{\mathrm{cr}}(\mathbb{L}')$. We just need to show $\tilde{g}(I) = 0$.

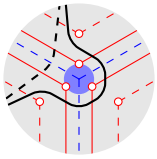

FIGURE 14. Extra splitting curves.

$\tilde{g}$ maps (60) to zero via either ϵ or k. For the handle slide, we first reduce to the case of a single standard arc. In each annulus component, draw another splitting curve close enough to the red curve but also away from the handle slide region. See the dashed red curve in Figure 14, where both sides of the handle slide are shown. Here, close enough means the diagram in the region between them consists of small segments of standard arcs and the segments of the handle slide. Now split along the dashed curves and apply the counit. Since the handle slide is sandwiched between the red curves, the counit for both sides of the handle slide are the same. We can also choose the height order so that the arc changed by the handle slide is at the bottom. This means if $\tilde{g}$ is invariant for the handle slide of a single standard arc, then by multiplying the rest of the diagram on the left, we prove the invariance for general diagrams. Up to symmetry, there is only one handle slide of standard arcs (with 4 combinations of states). By reinterpreting the calculations in Lemma 4.24, we obtain the invariance under $\tilde{g}$. Therefore, $\tilde{g}$ sends both types of generators of I to 0. □

5. A quantum trace map of triangulated 3-manifolds

In this section we give the promised definition of the quantum trace map (12) and prove its properties stated in Theorems 1.1 and 1.3.

5.1. **Quantum gluing module.** Let M be an oriented 3-manifold with an ideal triangulation $\mathcal{T}$. Let $\mathcal{H}_{\mathcal{T}} := (\Sigma_{\mathcal{T}}, \{A_f\}, \{B_e\})$ be the dual surface from Section 2.1. By construction, $\Sigma_{\mathcal{T}}$ split along all A-curves consists of a lantern $\mathbb{L}_j = \Sigma_{\mathcal{T}} \cap T_j$ for each tetrahedron T_j.

The quantum gluing module $\widehat{\mathcal{G}}(\mathcal{T})$ was explained in the introduction. By rearranging the order of quotients and tensor products, there is a presentation more compatible with splitting. Note that the Lagrangian equations only involve variables from the same tetrahedron. Thus, the quotient by Lagrangian can be taken before the tensor product, so

$$\widehat{\mathcal{G}}(\mathcal{T}) = \langle \text{edge} \rangle_R \backslash \Big(\bigotimes_{j=1}^{N} \mathbb{T} \langle \hat{z}_j, \hat{z}_j'' \rangle /_L \langle \text{Lagrangian} \rangle \Big) . \tag{74}$$

Using Theorem 4.26, for each tetrahedron T_j, we get an isomorphism

$$\widehat{\mathcal{G}}(\mathbb{L}) /_L \langle \hat{z} - \hat{y} \rangle \cong \mathbb{T} \langle \hat{z}_j, \hat{z}_j'' \rangle /_L \langle \text{Lagrangian} \rangle \tag{75}$$

sending $\hat{z} \mapsto \hat{z}_j$ and $\hat{z}'' \mapsto \hat{z}_j''$. Tensoring these together, we get another definition

$$\widehat{\mathcal{G}}(\mathcal{T}) = \langle \text{edge} \rangle_R \backslash \Big(\bigotimes_{j=1}^{N} \widehat{\mathcal{G}}(\mathbb{L}_j) /_L \langle \hat{z}_j - \hat{y}_j \rangle \Big) \tag{76}$$

where the generators of each copy $\widehat{\mathcal{G}}(\mathbb{L}_j)$ is now written with the index j.

Remark 5.1. We can extend the definition of $\widehat{\mathcal{G}}(\mathcal{T})$ to include the $\hat{y}$ variables by removing the quotient of ${}_L\langle \hat{z}_j - \hat{y}_j \rangle$. The results below all work with this extension.

Like the skein module, if the choices of R and q need to be shown, we will use the notation $\widehat{\mathcal{G}}_q(\mathcal{T}; R)$. As an example, the coordinate ring $\mathbb{C}[G_{\mathcal{T}}]$ of the gluing variety is $\widehat{\mathcal{G}}_1(\mathcal{T}; \mathbb{C})/\sqrt{0}$.

We have a universal coefficient property similar to (23).

Lemma 5.2. Suppose $r : R \to R'$ is a ring homomorphism and $r(q) = q'$. Then

$$\widehat{\mathcal{G}}_q(\mathcal{T}; R) \otimes_R R' \cong \widehat{\mathcal{G}}_{q'}(\mathcal{T}; R'). \tag{77}$$

Proof. The proof is the same as [Prz99, Proposition 2.2(4)]. The key here is that $\widehat{\mathcal{G}}$ is a quotient of a quantum torus, which is a free module. In particular, $\mathbb{T}_q(\mathcal{T}; R) \otimes_R R' = \mathbb{T}_{q'}(\mathcal{T}; R')$. Let $I_R = \ker(\mathbb{T}_q(\mathcal{T}; R) \twoheadrightarrow \widehat{\mathcal{G}}_q(\mathcal{T}; R))$, and define $I_{R'}$ similarly. Then we have exact sequences

$$\begin{array}{ccccccc} I_R \otimes_R R' & \longrightarrow & \mathbb{T}_q(\mathcal{T}; R) \otimes_R R' & \longrightarrow & \widehat{\mathcal{G}}_q(\mathcal{T}; R) \otimes_R R' & \longrightarrow & 0 \\ \downarrow & & \| & & \downarrow & & \\ I_{R'} & \longrightarrow & \mathbb{T}_{q'}(\mathcal{T}; R') & \longrightarrow & \widehat{\mathcal{G}}_{q'}(\mathcal{T}; R') & \longrightarrow & 0 \end{array} \tag{78}$$

Here, the top row is exact by the right exactness of the tensor product. A formal argument shows that the left vertical map is surjective. Then the five lemma proves (77). □

5.2. **Quantum trace map.** Starting from the dual surface $\mathcal{H}_{\mathcal{T}} := (\Sigma_{\mathcal{T}}, \{A_f\}, \{B_e\})$, instead of a cell structure, we can recover M from $\mathcal{H}_{\mathcal{T}}$ using a Heegaard-like process. By attaching 2-handles to the closed thickening $\Sigma_{\mathcal{T}} \times [-1, 1]$ along all $A_f \times \{-1\}$ and capping off spherical boundary components, we obtain the handlebody inside the surface $\Sigma_{\mathcal{T}}$. Then M is obtained by attaching 2-handles to all $B_e \times \{1\}$.

By Proposition 4.3, there is a surjective map $\mathcal{S}(\Sigma_{\mathcal{T}}) \twoheadrightarrow \mathcal{S}(M)$, and the kernel is generated by handle slides. Since the A-handles are attached to the bottom, the submodule ${}_L\langle A \rangle$ of A-handle slides is a left ideal in $\mathcal{S}(\Sigma_{\mathcal{T}})$. Similarly, the B-handle slides generate a right ideal $\langle B \rangle_R$. Thus, we get the isomorphism claimed in Proposition 1.2

$$\langle B \rangle_R \backslash \mathcal{S}(\Sigma_{\mathcal{T}}) / {}_L\langle A \rangle \xrightarrow{\cong} \mathcal{S}(M). \tag{79}$$

Define the quantum trace map $\widehat{\mathrm{tr}}_{\mathcal{T}} : \mathcal{S}(M) \to \widehat{\mathcal{G}}(\mathcal{T})$ using the following diagram.

$$\begin{array}{ccccc} \mathcal{S}(\Sigma_{\mathcal{T}}) & \xrightarrow{\Theta_A} & \bigotimes_{j=1}^N \mathcal{S}^{\mathrm{cr}}(\mathbb{L}_j) & \twoheadrightarrow & \bigotimes_{j=1}^N \widehat{\mathcal{G}}(\mathbb{L}_j) \\ \downarrow & \searrow^{\widetilde{\mathrm{tr}}_{\mathcal{T}}} & & & \downarrow \\ \mathcal{S}(M) & \dashrightarrow_{\widehat{\mathrm{tr}}^q_{\mathcal{T}}} & & & \widehat{\mathcal{G}}(\mathcal{T}) \end{array} \tag{80}$$

Here Θ_A is the splitting map along all A-circles. As before, q can be included like $\widehat{\mathrm{tr}}^q_{\mathcal{T}}$ if it is important.

Theorem 5.3. *The map $\widehat{\mathrm{tr}}_{\mathcal{T}} : \mathcal{S}(M) \to \widehat{\mathcal{G}}(\mathcal{T})$ is well-defined.*

Proof. Define the composition $\widetilde{\mathrm{tr}}_{\mathcal{T}}$ using the diagram. We need to show that $\widetilde{\mathrm{tr}}_{\mathcal{T}}({}_L\langle A\rangle) = 0$ and $\widetilde{\mathrm{tr}}_{\mathcal{T}}(\langle B\rangle_R) = 0$.

First consider the handle slide along A_f for some face f. To calculate the cut Θ_A, we need to isotope the handle slide region slightly to be disjoint from the curve A_f. Then after splitting, the handle slide becomes an identity in $\mathcal{S}^{\mathrm{cr}}(\mathbb{L})$ by Lemma 4.14. Thus, $\Theta_A({}_L\langle A\rangle) = 0$, so $\widetilde{\mathrm{tr}}_{\mathcal{T}}({}_L\langle A\rangle) = 0$ as well.

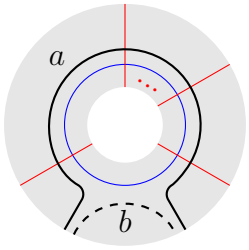

FIGURE 15. B-handle slide: $a = b$ in $\mathcal{S}(M)$.

Now look at the handle slide along B_e for some edge e. A neighborhood of B_e is shown in Figure 15, where the blue circle is B_e, and the red segments are parts of the A-circles. The black strands are part of link, and both sides of the handle slide are shown. There may be additional strands of the link in the region, but they are all below the strand in the figure. By definition, we split along the red A-circles and identify the components with the standard lantern $\mathbb{L}$ such that the blue B-arcs are the standard arcs. This means the punctures of the split are away from the B-circles. We use the convention where we omit the additional strands and consider the relations "at the top".

Start with the solid strand a in Figure 15. Except for the segments in the south, the arcs after splitting along the A-circles are standard arcs, which we can make to be higher than all other strands. By Lemma 4.23, if any of the standard arcs after splitting has opposite states, then the diagram is zero in $\widehat{\mathcal{G}}$. Therefore, any nonzero term has all $+$ or all $-$ states in the region in Figure 15. Define the following tangles in the surface after splitting.

$a_\mu =$ 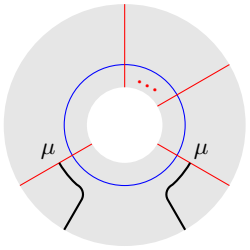

, $c =$ 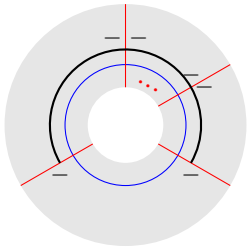

, $d =$ 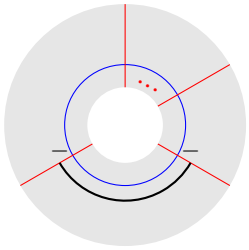

. (81)

Here, a_μ is a sum over the states of all endpoints not shown in the figure. Then by definition,

$$\widetilde{\mathrm{tr}}_{\mathcal{T}}(a) = c \cup a_- + c^{-1} \cup a_+. \tag{82}$$

Here, the $\cup$-product is performed before reduction to $\widehat{\mathcal{G}}(\mathcal{T})$. On the other hand, if we isotope b and impose height order as below,

$b =$ 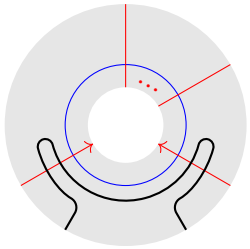 , (83)

we get

$\widetilde{\mathrm{tr}}_{\mathcal{T}}(b) =$  $= -q^{-2} d \cup a_+ - q^2 d^{-1} \cup a_-.$ (84)

We finish the proof by showing that the (quantized) edge equation imply $\widetilde{\mathrm{tr}}_{\mathcal{T}}(a) = \widetilde{\mathrm{tr}}_{\mathcal{T}}(b)$.

To do so, we first identify the edge equation with $d \cup c = -q^2$. By construction, different standard arcs do not end on the same boundary edge. Thus, $d \cup c$ consists of arcs that commute under $\cup$, so it is the Weyl-ordered product under $\cdot$, which is the monomial used in the edge equation.

Now we start from (82) and insert $1 = -q^{-2}(d \cup c)$ and its inverse,

$$\widetilde{\mathrm{tr}}_{\mathcal{T}}(a) = -q^2 (d^{-1} \cup c^{-1}) \cdot (c \cup a_-) - q^2 (d \cup c) \cdot (c^{-1} \cup a_+). \tag{85}$$

We would like to cancel c with its inverse. This can be done by rewriting the $\cdot$ using $\cup$. The correction factors in both terms are 1. This is because the terms in (82) are results of splitting. This means the endpoints and their states appear in pairs on matching boundary triangles. The same is true of $d \cup c$ and its inverse. Because of the orientation, the matching boundary triangles give opposite factors in (31). Therefore, in (85), we can replace $\cdot$ with $\cup$ without additional factors. Then after cancelling c with its inverse, we get $\widetilde{\mathrm{tr}}_{\mathcal{T}}(a) = \widetilde{\mathrm{tr}}_{\mathcal{T}}(b)$. This shows $\widetilde{\mathrm{tr}}_{\mathcal{T}}(\langle B \rangle_R) = 0$. □

5.3. **Classical limit.** Now we establish the classical limit, namely the commutativity of the diagram (13). This can be factored as follows.

$$\begin{array}{ccc}
\mathcal{S}_q(M; R_{\mathrm{univ}}) & \xrightarrow{\widehat{\mathrm{tr}}^q_{\mathcal{T}}} & \widehat{\mathcal{G}}_q(\mathcal{T}; R_{\mathrm{univ}}) \\
\downarrow{\scriptstyle \otimes \mathbb{C}} & & \downarrow{\scriptstyle \otimes \mathbb{C}} \\
\mathcal{S}_1(M; \mathbb{C}) & \xrightarrow{\widehat{\mathrm{tr}}^1_{\mathcal{T}}} & \widehat{\mathcal{G}}_1(\mathcal{T}; \mathbb{C}) \\
\downarrow{\scriptstyle /\sqrt{0}} & & \downarrow{\scriptstyle /\sqrt{0}} \\
\mathbb{C}[X^{\mathrm{Fr}}_M] & \xrightarrow{\mathrm{tr}_{\mathcal{T}}} & \mathbb{C}[G_{\mathcal{T}}]
\end{array} \tag{86}$$

The vertical map $\mathcal{S}_1(M; \mathbb{C}) \to \mathbb{C}[X^{\mathrm{Fr}}_M]$ comes from Lemma 4.2. The bottom map $\mathrm{tr}_{\mathcal{T}}$ is the classical trace map induced by $G_{\mathcal{T}} \to X^{\mathrm{Fr}}_M$ from Proposition 3.3.

Theorem 5.4. *The diagram (86) commutes.*

Proof. The top square commutes essentially by definition, so we focus on the bottom square.

As observed in [Lî18], in the stated skein algebra with $q = 1$, the element defined by a tangle is unchanged by crossing changes as well as height reordering on the boundary. This also means the stated skein algebra is commutative (for both $\cup$ and $\cdot$ since the correction factor in (31) is 1). This is also passed on to the various quotients, and the diagram (80) that defines $\widehat{\mathrm{tr}}^1_{\mathcal{T}}$ is a commutative diagram of algebras and algebra maps.

This discussion shows that $\widehat{\mathrm{tr}}^1_{\mathcal{T}}$ is an algebra homomorphism, so we can check the bottom square on algebra generators of $\mathcal{S}_1(M;\mathbb{C})$. Since $\mathcal{S}_1(M;\mathbb{C})$ is a quotient of $\mathcal{S}_1(\Sigma_{\mathcal{T}};\mathbb{C})$, closed curves on $\Sigma_{\mathcal{T}}$ with vertical framing generates $\mathcal{S}_1(M;\mathbb{C})$. Such a curve is homotopic to a curve K on the smooth 1-skeleton $\mathfrak{T}^{(1)}$ defined in Section 3.2. Thus, it is sufficient to consider curves K of this form.

To calculate $\widehat{\mathrm{tr}}^1_{\mathcal{T}}(K)$, we need to calculate the splitting $\Theta_A(K)$. By definition, K is transverse to all splitting curves A_f. Then (39) can be applied to K since heights do not matter for $q = 1$. Choose an arbitrary orientation of K and write $K = m^1 m^2 \cdots m^k$ as a concatenation of edges of $\mathfrak{T}^{(1)}$. Then

$$\Theta_A(K) = \sum_{s_1,\dots,s_k=\pm 1} m^1_{s_1 s_2} m^2_{s_2 s_3} \cdots m^k_{s_k s_1} = \mathrm{tr}(\hat{M}^1 \hat{M}^2 \cdots \hat{M}^k). \tag{87}$$

Here, we used the notation for arcs with states assigned from Section 4.6, and

$$\hat{M}^i = \begin{pmatrix} m^i_{++} & m^i_{+-} \\ m^i_{-+} & m^i_{--} \end{pmatrix} \tag{88}$$

is a 2×2 matrix over $\mathcal{S}_1^{\mathrm{cr}}(\mathbb{L};\mathbb{C})$, which is mapped to $\widehat{\mathcal{G}}_1(\mathbb{L};\mathbb{C})$. If the arc m^i is an α edge, then

$$m^i_{st} = \quad \begin{matrix} s \\ t \end{matrix}, \qquad \hat{M}^i = \begin{pmatrix} 0 & 1 \\ -1 & 0 \end{pmatrix}. \tag{89}$$

If the arc m^i is a β edge, then

$$m^i_{st} = \quad \begin{matrix} t \\ s \end{matrix}, \qquad \hat{M}^i = \begin{pmatrix} \mathbf{i} & 0 \\ 1 & -\mathbf{i} \end{pmatrix}. \tag{90}$$

Finally, if the arc m^i is a γ edge, then it is a standard arc of the lantern. By definitions (60) and (63), after reduced to $\widehat{\mathcal{G}}_1(\mathbb{L};\mathbb{C})$,

$$\hat{M}^i = \begin{pmatrix} \hat{z}^{-1} & 0 \\ 0 & \hat{z} \end{pmatrix}. \tag{91}$$

Let M^i be $\hat{M}^i$ mod nilradical, which removes the hat on $\hat{z}$. Then M^i are exactly the matrices in Proposition 3.3, so

$$\mathrm{tr}_{\mathcal{T}}(t_K) = \mathrm{tr}(M^1 M^2 \cdots M^k) = \widehat{\mathrm{tr}}^1_{\mathcal{T}}(K) \text{ mod nilradical.} \tag{92}$$

Thus, the bottom square commutes. □

5.4. **Chebyshev-Frobenius map.** In this section we discuss the quantum trace map at roots of unity. To do so, we need to recall the Chebyshev-Frobenius map on the skein module and on the quantum torus. $R = \mathbb{C}$ throughout this section and are omitted from the notations.

Given a framed knot $K \subset M$, let the *framed power* $K^{(n)} \subset M$ be the link consisting of n parallel copies of K, obtained by small translation in the direction of the framing. For a polynomial $f(x) = \sum_{i=0}^{n} a_i x^i$, the *threading* of K by f is defined as

$$K^{(f)} = \sum_{i=0}^{n} a_i K^{(i)} \in \mathcal{S}(M). \tag{93}$$

More generally, the threading of a link $L = K_1 \cup \cdots \cup K_\ell$ by f is defined as a "linear extension" of applying $f(x)$ to every component of L

$$L^{(f)} = \sum_{i_1,\dots,i_\ell=0}^{n} a_{i_1} \cdots a_{i_\ell} K_1^{(i_1)} \cup \cdots \cup K_\ell^{(i_\ell)} \in \mathcal{S}(M). \tag{94}$$

When q is a root of unity, threading by Chebyshev polynomials has special properties. The Chebyshev polynomial $T_n(x) \in \mathbb{Z}[x]$ is the family of polynomials given by

$$T_0(x) = 2, \qquad T_1(x) = x, \qquad T_n(x) = xT_{n-1}(x) - T_{n-2}(x), \quad n \geq 2. \tag{95}$$

Suppose $\zeta \in \mathbb{C}$ such that ζ^4 is a primitive N-th root of unity. Let $\varepsilon = \zeta^{N^2}$. Then threading links by T_N defines a map

$$\Phi_\zeta : \mathcal{S}_\varepsilon(M) \to \mathcal{S}_\zeta(M). \tag{96}$$

This is the *Chebyshev homomorphism* introduced by [BW16], and it can be defined in the context of punctured bordered surfaces. Note the framed power $a^{(N)}$ makes sense for a (framed, stated) arc a over Σ.

Theorem 5.5 ([BL22, Corollary 4.7])**.** *Fix a punctured bordered surface Σ. Then there exists a unique algebra homomorphism $\Phi_\zeta : \mathcal{S}_\varepsilon(\Sigma) \to \mathcal{S}_\zeta(\Sigma)$ (using the $\cup$-product) such that*

$$\Phi_\zeta(a) = a^{(N)} \quad \text{if } a \text{ is an arc}, \qquad \Phi_\zeta(K) = K^{(T_N)} \quad \text{if } K \text{ is a knot}. \tag{97}$$

Let e be an ideal arc on Σ and Σ_e be the splitting of Σ along e. Then Φ_ζ is compatible with splitting homomorphisms, that is, the following diagram commutes.

$$\begin{array}{ccc} \mathcal{S}_\varepsilon(\Sigma) & \xrightarrow{\Theta_e} & \mathcal{S}_\varepsilon(\Sigma_e) \\ \downarrow{\scriptstyle \Phi_\zeta} & & \downarrow{\scriptstyle \Phi_\zeta} \\ \mathcal{S}_\zeta(\Sigma) & \xrightarrow{\Theta_e} & \mathcal{S}_\zeta(\Sigma_e) \end{array} \tag{98}$$

We next recall the analogous map, the *Frobenius homomorphism* on a quantum torus. It is given by

$$\Phi_\zeta^{\mathbb{T}} : \mathbb{T}_\varepsilon\langle x_1, \dots, x_k\rangle \to \mathbb{T}_\zeta\langle x_1, \dots, x_k\rangle, \qquad \Phi_\zeta^{\mathbb{T}}(x_i) = x_i^N. \tag{99}$$

This map does not require ζ to be a root of unity, and N could be arbitrary (but still with $\varepsilon = \zeta^{N^2}$). However, it is only relevant to us when ζ and N are as before.

Lemma 5.6. The Frobenius homomorphism for $\mathbb{T}\langle \hat{z}, qz''\rangle$ maps the Lagrangian to the Lagrangian.

The Frobenius homomorphism for $\mathbb{T}(\mathcal{T})$ maps the edge equations to the edge equations.

Thus, the Frobenius homomorphisms induce maps

$$\varphi_\zeta : \widehat{\mathcal{G}}_\varepsilon(\mathbb{L}) \to \widehat{\mathcal{G}}_\zeta(\mathbb{L}), \qquad \varphi_\zeta : \widehat{\mathcal{G}}_\varepsilon(\mathcal{T}) \to \widehat{\mathcal{G}}_\zeta(\mathcal{T}). \tag{100}$$

Proof. For the Lagrangian equations, we use the following form of the q-binomial theorem at roots of unity: if $XY = \omega YX$ for a root of unity ω with order N, then the quantum binomial theorem and the vanishing of the quantum binomial at roots of unity implies that

$$(X+Y)^N = X^N + Y^N. \tag{101}$$

Apply this to $X = \hat{z}^{-2}$, $Y = (\hat{z}'')^2$, and $\omega = \zeta^4$, we get

$$\Phi^{\mathbb{T}}_\zeta(\hat{z}^{-2} + (\hat{z}'')^2) = \hat{z}^{-2N} + (\hat{z}'')^{2N} = (\hat{z}^{-2} + (\hat{z}'')^2)^N = 1. \tag{102}$$

For the edge equations, this is a standard algebraic calculation. First, a simple check shows that

$$(-\zeta^2)^N = -\varepsilon^2. \tag{103}$$

Now, $\Phi^{\mathbb{T}}_\zeta$ sends a Weyl-ordered monomial to its N-th power, so (edge) $= -\varepsilon^2$ is sent to $(\text{edge})^N = -\varepsilon^2$, which is the correct equation by (103).

After verifying that all calculations are compatible with multiplication on the appropriate sides, we get the map φ_ζ. □

As mentioned in Remark 4.11, here we actually need to be careful about the choice of the 4-th root of unity $\mathbf{i}$. By (103),

$$\mathbf{i}' = (\mathbf{i}\zeta)^N/\varepsilon \tag{104}$$

is a primitive 4-th root of unity, but it could be either $\pm\mathbf{i}$. We use $\mathbf{i}$ for $q = \zeta$ and $\mathbf{i}'$ for $q = \varepsilon$.

In the rest of the section we give a proof of Theorem 1.3. Recall that to split a surface along a closed curve, we remove 3 points and split along the three ideal arcs. Let $\Sigma'_\mathcal{T}$ be $\Sigma_\mathcal{T}$ with three points removed for each A-curve, and let Θ'_A be the splitting along ideal A-arcs for $\Sigma'_\mathcal{T}$. Then by definition (43), the following diagram commutes.

$$\begin{array}{ccc} \mathcal{S}(\Sigma'_\mathcal{T}) & \xrightarrow{\Theta'_A} & \bigotimes_{j=1}^N \mathcal{S}(\mathbb{L}_j) \\ \downarrow & & \downarrow \\ \mathcal{S}(\Sigma_\mathcal{T}) & \xrightarrow{\Theta_A} & \bigotimes_{j=1}^N \mathcal{S}^{\mathrm{cr}}(\mathbb{L}_j) \end{array} \tag{105}$$

Expand the diagram (17) using the definition of the quantum trace map and replace Θ_A by Θ'_A using the diagram above. Then we need to show that the following diagram commutes.

$$\begin{array}{ccccccccc} \mathcal{S}_\varepsilon(M) & \twoheadleftarrow & \mathcal{S}_\varepsilon(\Sigma'_\mathcal{T}) & \xrightarrow{\Theta'_A} & \bigotimes_{j=1}^N \mathcal{S}_\varepsilon(\mathbb{L}_j) & \twoheadrightarrow & \bigotimes_{j=1}^N \widehat{\mathcal{G}}_\varepsilon(\mathbb{L}_j) & \longrightarrow & \widehat{\mathcal{G}}_\varepsilon(\mathcal{T}) \\ \downarrow{\scriptstyle \Phi_\zeta} & & \downarrow{\scriptstyle \Phi_\zeta} & & \downarrow{\scriptstyle \otimes\Phi_\zeta} & & \downarrow{\scriptstyle \otimes\varphi_\zeta} & & \downarrow{\scriptstyle \varphi_\zeta} \\ \mathcal{S}_\zeta(M) & \twoheadleftarrow & \mathcal{S}_\zeta(\Sigma'_\mathcal{T}) & \xrightarrow{\Theta'_A} & \bigotimes_{j=1}^N \mathcal{S}_\zeta(\mathbb{L}_j) & \twoheadrightarrow & \bigotimes_{j=1}^N \widehat{\mathcal{G}}_\zeta(\mathbb{L}_j) & \longrightarrow & \widehat{\mathcal{G}}_\zeta(\mathcal{T}) \end{array} \tag{106}$$

The first and the last squares commute essentially by definition. The second square commutes by Theorem 5.5. For the remaining third square, we show that it commutes on each tensor factor. By definition, if a is a simple arc diagram whose endpoints are on different boundary edges, then the framed power $a^{(N)}$ agrees with the algebraic power a^N. Then by the choice (104), Φ_ζ respects the corner reductions (29) and (32), so we can replace $\mathcal{S}_\bullet(\mathbb{L}_j)$ with $\mathcal{S}^{\mathrm{cr}}_\bullet(\mathbb{L}_j)$ in the diagram. Then by Lemma 4.22, $\mathcal{S}^{\mathrm{cr}}_\bullet(\mathbb{L})$ is spanned by products of arcs with endpoints on different boundary edges, so Φ_ζ is given by the algebraic power again. Moreover, each arc is either a generator of $\widehat{\mathcal{G}}(\mathbb{L}_j)$ or 0, so Φ_ζ matches φ_ζ on this spanning set. This proves the commutativity of the third square.

This completes the proof of Theorem 1.3. □

6. Computational aspects

In this section we discuss how to compute the quantum trace map (12) using the methods of `SnapPy`, following the pioneering ideas of Thurston. This method uses as input triangulations of 3-manifolds [CDGW]. The data of a triangulation $\mathcal{T}$ encoded in `SnapPy` allows one to define the lantern surface and to describe the peripheral curves on it. In a future addition to these methods, one may add framed links in the complement of a knot and trace them to the ideal triangulation of the knot complement, and then to the lantern surface giving an effective computation of the quantum trace map.

6.1. Cusp diagram and dual surface.

In this section we discuss how to obtain the lantern surface from an ideal triangulation encoded in `SnapPy`.

Given an ideal triangulation $\mathcal{T}$ of M, the cell decomposition $\mathfrak{T}$ using double truncation restricts to a cell decomposition $\mathfrak{T}_\partial$ of the boundary ∂M. From Figure 5, we see that ∂M is glued from the vertex hexagons $(\gamma^{-1}\beta)^3$, the base polygons of edge prisms γ^n, and the circles β^2.

In `SnapPy`, the tetrahedra in ideal triangulations are only truncated once at the vertices but not the edges. In this case, the boundary ∂M is given by a triangulation λ. We can easily truncate λ to obtain $\mathfrak{T}_\partial$. The triangles of λ become the vertex hexagons of $\mathfrak{T}_\partial$, and the corners of the triangles correspond to γ edges. The truncated edges of λ can be doubled into β edges if needed. See Figure 16.

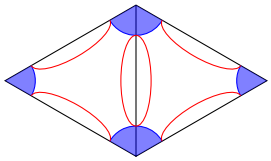

Figure 16. The truncated triangulation of the cusp.

Now compare ∂M with the dual surface $\Sigma_\mathcal{T}$, shown in Figure 6. They share the vertex hexagons and the β^2 circles. While ∂M has the bases of edge prisms, $\Sigma_\mathcal{T}$ has the sides of the edge prisms, which are the annuli between parallel B-curves. This shows that ∂M can be obtained from $\Sigma_\mathcal{T}$ by surgery along all B-curves.

Conversely, we can reverse the surgery. This also recovers the decorations on $\Sigma_\mathcal{T}$ with some additional bookkeeping which `SnapPy` does. By definition, the reverse surgery truncates the

vertices of λ and pair the boundary circles by gluing in annuli. Clearly, the B-curves are just the boundary circles after truncation. The A-curves are homotopic to $(\alpha\beta)^3$ in the 1-skeleton $\mathfrak{T}^{(1)}$. α edges are just transverse arcs of the inserted annuli, and β edges are homotopic to truncated edges of λ. Note the ends of edges in λ correspond to ends of edges in $\mathcal{T}$. `SnapPy` keeps track of this correspondence, which determines which triples of truncated edges connect to form the A-circles.

It is convenient to describe $\Sigma_{\mathcal{T}}$ by splitting into lanterns so that the diagrams are planar and that the quantum trace can be calculated. This can be obtained from λ by

(1) truncating the vertices to create the γ edges,
(2) splitting along the truncated edges, resulting in the vertex hexagons, and
(3) gluing the hexagons along γ edges, which become standard arcs on the lantern.

In step (2), the pairings of the truncated edges after splitting needs to be recorded so that the lanterns can glue back together.

`SnapPy` also calculates the meridian and longitude, given as cycles in the dual 1-skeleton of λ. This means the curves intersect edges of λ transversely and do not go through vertices of λ. Then the steps above also draw the curves on the lanterns.

The second author has implemented the lantern surface of a `SnapPy` triangulation as a python module.

6.2. **Example: The 4_1 knot.** In this section we illustrate the discussion of the previous section, and the computation of the quantum trace map with the default triangulation $\mathcal{T}$ of the 4_1 knot with isometry signature `cPcbbbiht_BaCB`. This is a triangulation with two tetrahedra T_0 and T_1 shown in Figure 17 using the convention from Figure 1. There are 4 face pairings labeled A,B,C,D.

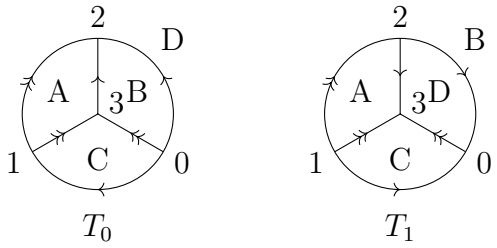

FIGURE 17. `SnapPy` triangulation of the 4_1 knot.

The triangulation λ of the cusp calculated by `SnapPy` is shown in Figure 18 after truncation. The triangle near vertex i in T_j is indexed by $i + 4j$. The edge numbering is also included for the lantern diagram later. The labels 1,2 at truncated vertices refer to the edges of $\mathcal{T}$ corresponding to single or double arrows in Figure 17. The meridian μ and longitude λ (simplified by twisting twice around μ) of the 4_1 knot are also included.

Now we can convert the cusp diagram to the dual surface $\Sigma_{\mathcal{T}}$ by gluing the truncated vertices of the cusp. To make sure the truncated edges of the cusp match correctly to form the A-circles, we mark the arcs around the 01 and 13 edges in T_0 with arrows in Figure 17, which can be continued to obtain all other pairings.

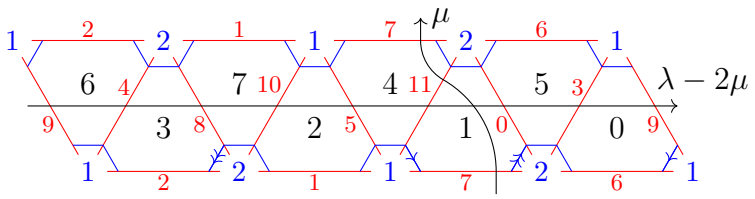

FIGURE 18. Cusp diagram of the 4_1 knot.

Next, we split $\Sigma_{\mathcal{T}}$ along A-circles to obtain lantern diagrams. We can determine all pairings of the blue edges using the markings in Figure 18 or using additional `SnapPy` data not shown in the figure. After splitting the red edges and gluing the blue edges, we obtain Figure 19. Here, the orientations of the blue standard arcs are induced from Figure 18.

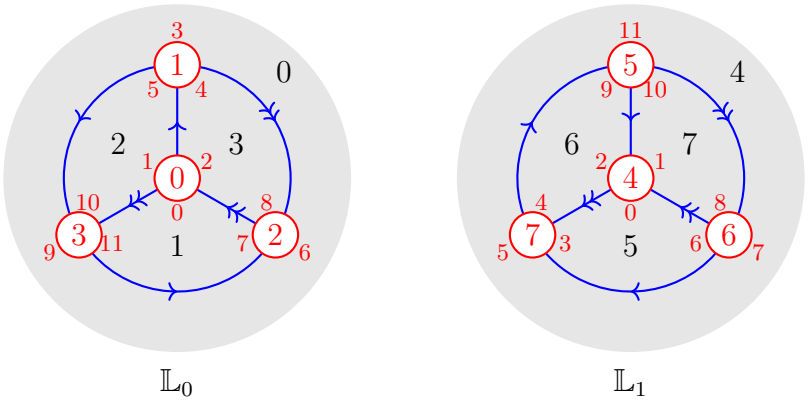

FIGURE 19. Lantern diagram for the 4_1 knot.

The meridian μ and the longitude λ are shown in the subsequent Figures 20 and 21, where the labels are omitted to avoid clutter.

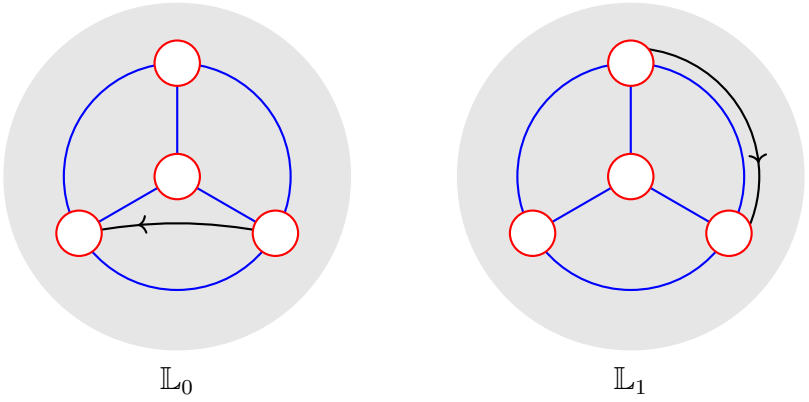

FIGURE 20. Meridian of the 4_1 knot.

Finally, we calculate $\widehat{\mathrm{tr}}_{\mathcal{T}}(\mu)$ as an example. To interpret Figure 20 as the diagram of $\mu \in \mathcal{S}(\Sigma_{\mathcal{T}})$ after splitting, we need to add punctures to the boundaries of $\mathbb{L}_j$. The exact

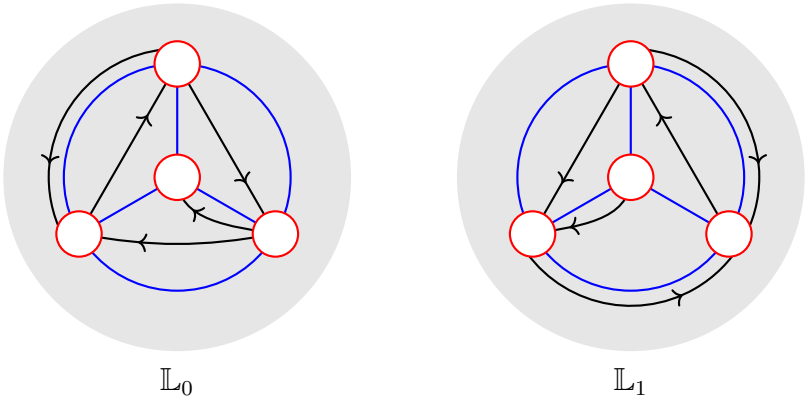

FIGURE 21. Longitude of the 4_1 knot.

positions of the punctures do not matter, as long as they are consistent between lanterns. We make the choice that the punctures on edges 7 and 11 are close to edges 6 and 9 respectively. This makes the arc $\mu^1 = \mu \cap \mathbb{L}_1$ standard, but the arc $\mu^0 = \mu \cap \mathbb{L}_0$ is not. In the state sum of the splitting, if the endpoints of μ^1 are assigned opposite states, then the diagram is zero in $\widehat{\mathcal{G}}(\mathbb{L}_1)$. Thus,

$$\widehat{\mathrm{tr}}_{\mathcal{T}}(\mu) = \sum_{s\in\{\pm\}} \mu^0_{ss} \otimes \mu^1_{ss}. \tag{107}$$

To express this in terms of quantized shape variables, we adopt the convention that $\hat{z}_j$ is associated to the 01 edge in T_j. In lantern diagrams, it corresponds to the standard arc connecting boundary circles 2,3 (shifted by $4j$). In this convention, $\mu^1_{ss} = (\hat{z}''_1)^{-s}$. For μ^0_{ss}, we can use Corollary 4.13 to twist it into standard arcs, giving $\mu^0_{ss} = \hat{z}^s_0$. Therefore,

$$\widehat{\mathrm{tr}}_{\mathcal{T}}(\mu) = \hat{z}_0(\hat{z}''_1)^{-1} + \hat{z}_0^{-1}\hat{z}''_1. \tag{108}$$

Acknowledgements. The authors wish to thank Francis Bonahon, Tudor Dimofte and Thang Lê for enlightening conversations.

APPENDIX A. PROOF OF THEOREM 4.18

Throughout this section, Σ is a surface with triangular boundary. All diagrams are positively ordered in this section, so the height order will be omitted.

The only nontrivial part is that ϕ_a is bijective. We do so by identifying a basis of $\mathcal{S}^{\mathrm{cr}}(\mathbb{A})$. Draw the standard annulus as in Figure 22, where the top and the bottom are identified. The dashed (ideal) arc is determined by the choice of a, and it will be used to describe the basis.

We say a tangle diagram on $\mathbb{A}$ is *normal* if it is in general position with the dashed arc. A normal isotopy is an isotopy within the class of normal diagrams. Then two normal isotopy classes of tangle diagrams represent isotopic tangles if and only if they are related by the

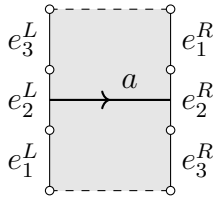

FIGURE 22. Labelling the standard annulus.

Reidemeister moves and the following moves

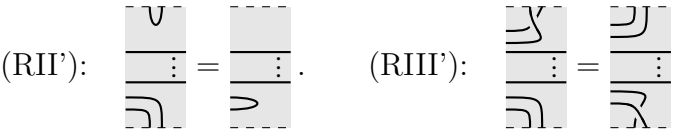

(109)

They are related by isotopies of $\mathbb{A}$, but not as normal diagrams. Let A be the set of normal isotopy classes of tangle diagrams on $\mathbb{A}$. Then the set of isotopy class of tangles is equivalent to the quotient of A by (framed) Reidemeister moves and RII', RIII'.

Let RA denote the free R-module spanned by A. RA has a product structure by stacking with coefficients just like (31). Of course, we only need the left action induced by the product.

Recall the linear diamond lemma from [SW07]. Let $S \subset A \times RA$, and write $a \to b$ for $(a,b) \in S$. Elements of S are called reduction rules on A. Define (S) as the R-submodule spanned by $\{a - b \in RA \mid a \to b\}$.

For $x, y \in RA$ with $x = \sum_i r_i a_i$ where $r_i \in R$ and $a_i \in A$, write $x \rightsquigarrow y$ if there exists a j such that $r_j \neq 0$ and $y = r_j b + \sum_{i \neq j} r_i a_i$ where $a_j \to b$. Finally, let $x \succeq y$ if $x = y$ or if there exists a sequence $x_0 \rightsquigarrow x_1 \cdots \rightsquigarrow x_n$ with $x_0 = x$, $x_n = y$. Clearly, (S) contains all $x - y$ with $x \succeq y$.

A set of reduction rules on A is called *locally confluent* if for any $a \in A$ and $b, c \in RA$ with $a \to b, a \to c$, there exists $v \in RA$ such that $b \succeq v$ and $c \succeq v$. An element $a \in A$ is *irreducible* if the only $b \in RA$ with $a \succeq b$ is $b = a$. Let $A_{\text{irr}} \subset A$ be the subset of irreducible elements.

The following result is a combination of Theorems 2.2 and 2.3 in [SW07].

Theorem A.1. *Let* $\deg : A \to J$ *be a map to a well-ordered set* J*, and let* $A_j = \{a \in A : \deg(a) < j\}$*. Suppose* S *is a locally confluent set of reduction rules on* A *such that for any* $a \to b$ *with* $\deg(a) = j$*,* $b \in RA_j$*. Then the map*

$$RA_{\text{irr}} \hookrightarrow RA \twoheadrightarrow RA/(S) \tag{110}$$

is an isomorphism.

Define the following set S of reduction rules on A.

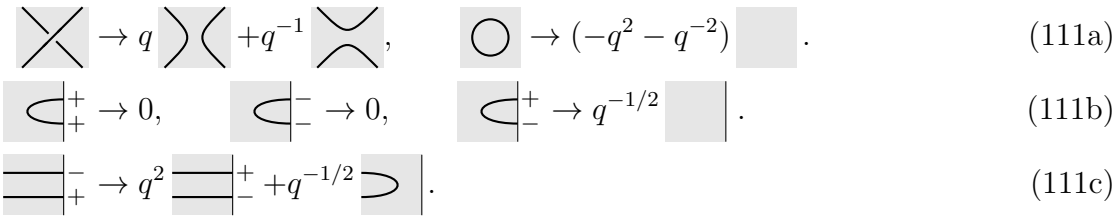

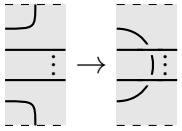
(111d)

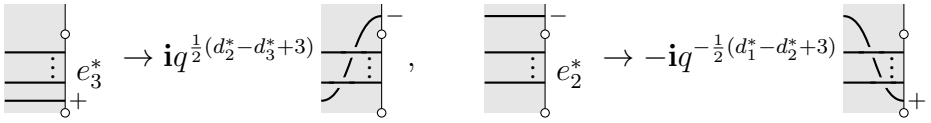
(111e)

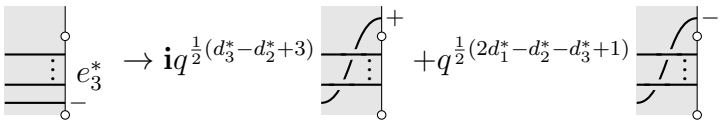
(111f)

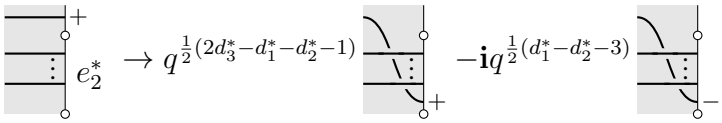
(111g)

Here, d_i^* is the grading on the edge e_i^* for $* = L, R$ and $i = 1, 2, 3$. Note (111a)–(111c) are taken from the proof of [LÎ18, Theorem 2.11] (cited here as Theorem 4.8). (111d)–(111g) are from Corollary 4.13 and Lemma 4.14.

Lemma A.2. The natural map $RA \to \mathcal{S}^{\mathrm{cr}}(\mathbb{A})$ descends to an isomorphism $RA/(S) \to \mathcal{S}^{\mathrm{cr}}(\mathbb{A})$.

Proof. The set of isotopy classes of tangles on $\mathbb{A}$ is the quotient of A by Reidemeister moves and RII', RIII'. Therefore, $\mathcal{S}^{\mathrm{cr}}(\mathbb{A}) = RA/I$ where I is the left ideal generated by Reidemeister moves, RII', RIII', (1)–(25), (29), and (32). Thus, we need to prove that $I = (S)$.

First we check that (S) is a left ideal in RA. This would be completely trivial if the product is simply stacking. The coefficients introduced by (31) requires some work for (111e)–(111g), but it is still straightforward.

By construction, all elements of (S) are 0 in $\mathcal{S}^{\mathrm{cr}}(\mathbb{A})$. Thus, $(S) \subset I$. To show the reverse inclusion, we need to reduce the generators of I to 0 using S. For Reidemeister moves, this is well-known; see e.g., [Kau87]. For RII', apply (111d) and Reidemeister moves. For RIII', after resolving the crossing, the two sides are related by an RII' move. (1), (2), (24), and (25) correspond to (111a)–(111c). For (29) and (32), they each come in 6 flavors, one for each puncture of $\mathbb{A}$. The opposite sides have the same reduction rules, so we only need to consider 3. Direct calculation shows they indeed have the correct reductions. □

Lemma A.3. The set S of reduction rules is locally confluent.

Proof. Define the support of the reduction moves to be the following closed subsets of $\mathbb{A}$:

- the crossing in the first move of (111a),
- the disk bounded by the loop in the second move of (111a),
- the disk bounded by the returning arc and part of $\partial\mathbb{A}$ in each move of (111b),
- the interval between the endpoints in (111c),
- the nontrivial loop through the intersection with the dashed arc in (111d), and
- the boundary triangle in each move of (111e)–(111g).

Let $a \in A$ be a diagram where two reduction rules $s_1, s_2 \in S$ apply. If the support of the reductions are disjoint, then it is easy to see that s_2 applies to the s_1-reduction and vice

versa. Moreover, when both reductions are applied, the result is independent of the order. Therefore, we only need to consider the case when the supports intersect. In addition, [LÎ18, Lemma 2.10] already proved that (111a)–(111c) are confluent. Thus, the remaining cases are

(1) (111b) or (111c) with (111e)–(111g).
(2) Among (111e)–(111g).

In (1), if the lower endpoint of (111b) or (111c) is not the one modified by (111e)–(111g), then the confluence is the same as the disjoint support case. There are 8 cases left to check: when the components of (111b) or (111c) are the lowest on e_1^* or e_3^*. Here we check one case. The rest are similar.

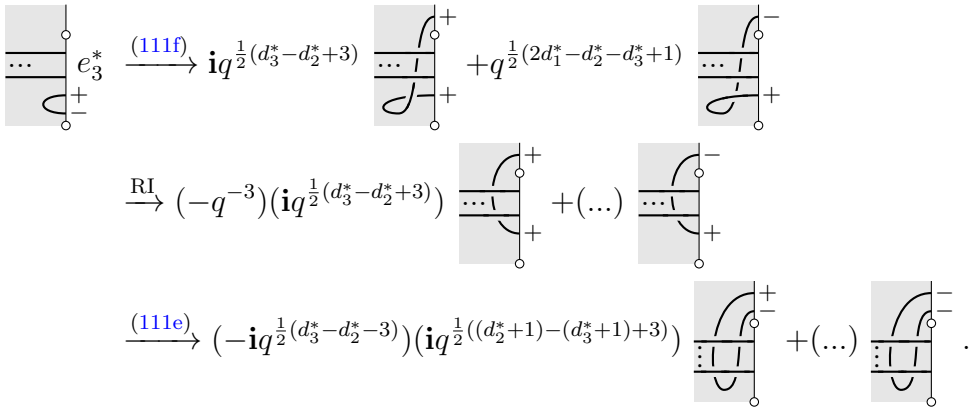

After RII and (111b), this agrees with the alternative reduction by applying (111b) first.

In (2), the overlaps are of the following form

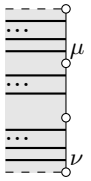

. (112)

Similar to the disjoint overlap case, the two reductions can be applied in any order, but the coefficients and the diagrams are different depending on the order. After some careful calculations, the reduction agree after some applications of (111a)–(111c) on e_2^*. □

Proof that ϕ_a is bijective. Define the degree $\deg = (\deg_1, \deg_2) : A \to \mathbb{N}^2$. $\deg_1$ is the total number of intersections with $e_{1,3}^*$ and the dashed arc. $\deg_2$ is the degree defined in the proof of [LÎ18, Lemma 2.10]. We do not need the exact definition. All we need are the following results:

- $\deg_2$ is decreased by (111a)–(111c).
- $\deg_2(a) = 0 \Leftrightarrow a$ is irreducible with respect to (111a)–(111c) $\Leftrightarrow a$ represents a basis element of $\mathcal{S}(\mathbb{A})$ in Theorem 4.8 with $\mathfrak{o}$ positive.

We use the lexicographical order on $\mathbb{N}^2$. Since (111a)–(111c) do not increase $\deg_1$, the first fact above shows they decrease deg. For the rest, they all decrease $\deg_1$ by 1, so they decrease deg as well. Thus, deg satisfies the condition in Theorem A.1. The local confluence is proved in Lemma A.3. By Theorem A.1, $RA/(S)$, naturally identified with $\mathcal{S}^{\mathrm{cr}}(\mathbb{A})$ by Lemma A.2,

is a free R-module with a basis given by the irreducible diagrams. The irreducible diagrams are basis elements of $\mathcal{S}(\mathbb{A})$ with no intersection with the dashed arc or endpoints on $e^*_{1,3}$. Such diagrams are contained in a neighborhood of a after normal isotopy, and they match the basis of $\mathcal{S}(\mathbb{B}) \cong \mathcal{O}_{q^2}(\mathrm{SL}_2)$ via ϕ_a. Therefore, ϕ_a is bijective. □

References

[AGLR] Prarit Agarwal, Dongmin Gang, Sangmin Lee, and Mauricio Romo, *Quantum trace map for 3-manifolds and a 'length conjecture'*, Preprint 2022, arXiv:2203.15985.

[Bar99] John Barrett, *Skein spaces and spin structures*, Math. Proc. Cambridge Philos. Soc. **126** (1999), no. 2, 267–275.

[BL22] Wade Bloomquist and Thang T.Q. Lê, *The Chebyshev-Frobenius homomorphism for stated skein modules of 3-manifolds*, Math. Z. **301** (2022), no. 1, 1063–1105.

[Bul97] Doug Bullock, *Rings of* $\mathrm{SL}_2(\mathbf{C})$*-characters and the Kauffman bracket skein module*, Comment. Math. Helv. **72** (1997), no. 4, 521–542.

[BW11] Francis Bonahon and Helen Wong, *Quantum traces for representations of surface groups in* $\mathrm{SL}_2(\mathbb{C})$, Geom. Topol. **15** (2011), no. 3, 1569–1615.

[BW16] ———, *Representations of the Kauffman bracket skein algebra I: invariants and miraculous cancellations*, Invent. Math. **204** (2016), no. 1, 195–243.

[CDGW] Marc Culler, Nathan Dunfield, Matthias Goerner, and Jeffrey Weeks, *SnapPy, a computer program for studying the geometry and topology of* 3*-manifolds*, Available at http://snappy.computop.org (version 3.1.1).

[CL22] Francesco Costantino and Thang T.Q. Lê, *Stated skein algebras of surfaces*, J. Eur. Math. Soc. (JEMS) **24** (2022), no. 12, 4063–4142.

[Dim13] Tudor Dimofte, *Quantum Riemann surfaces in Chern-Simons theory*, Adv. Theor. Math. Phys. **17** (2013), no. 3, 479–599.

[GGZ15] Stavros Garoufalidis, Matthias Goerner, and Christian Zickert, *Gluing equations for* $\mathrm{PGL}(n,\mathbb{C})$*-representations of 3-manifolds*, Algebr. Geom. Topol. **15** (2015), no. 1, 565–622.

[GW89] Kenneth Goodearl and Robert Warfield, *An introduction to noncommutative Noetherian rings*, London Mathematical Society Student Texts, vol. 16, Cambridge University Press, Cambridge, 1989.

[Kau87] Louis Kauffman, *State models and the Jones polynomial*, Topology **26** (1987), no. 3, 395–407.

[Lî5] Thang T.Q. Lê, *On Kauffman bracket skein modules at roots of unity*, Algebr. Geom. Topol. **15** (2015), no. 2, 1093–1117.

[Lî8] ———, *Triangular decomposition of skein algebras*, Quantum Topol. **9** (2018), no. 3, 591–632.

[LY] Thang T.Q. Lê and Tao Yu, *Quantum traces for* SL_n*-skein algebras*, Preprint 2023, arXiv:2303.08082.

[LY22] ———, *Quantum traces and embeddings of stated skein algebras into quantum tori*, Selecta Math. (N.S.) **28** (2022), no. 4, Paper No. 66, 48.

[Maj95] Shahn Majid, *Foundations of quantum group theory*, Cambridge University Press, Cambridge, 1995.

[NZ85] Walter Neumann and Don Zagier, *Volumes of hyperbolic three-manifolds*, Topology **24** (1985), no. 3, 307–332.

[Prz91] Józef Przytycki, *Skein modules of* 3*-manifolds*, Bull. Polish Acad. Sci. Math. **39** (1991), no. 1-2, 91–100.

[Prz99] ———, *Fundamentals of Kauffman bracket skein modules*, Kobe J. Math. **16** (1999), no. 1, 45–66.

[SW07] Adam Sikora and Bruce Westbury, *Confluence theory for graphs*, Algebr. Geom. Topol. **7** (2007), 439–478.

[Thu97] William Thurston, *Three-dimensional geometry and topology. Vol. 1*, Princeton Mathematical Series, vol. 35, Princeton University Press, Princeton, NJ, 1997, Edited by Silvio Levy, http://msri.org/publications/books/gt3m.

[Tur88] Vladimir Turaev, *The Conway and Kauffman modules of a solid torus*, Zap. Nauchn. Sem. Leningrad. Otdel. Mat. Inst. Steklov. (LOMI) **167** (1988), no. Issled. Topol. 6, 79–89, 190.

International Center for Mathematics, Department of Mathematics, Southern University of Science and Technology, Shenzhen, China
http://people.mpim-bonn.mpg.de/stavros
Email address: stavros@mpim-bonn.mpg.de

Shenzhen International Center for Mathematics, Southern University of Science and Technology, 1088 Xueyuan Avenue, Shenzhen, Guangdong, China
Email address: yut6@sustech.edu.cn